

1 Global Evaluation of the Ecosystem Demography Model (ED 2 v3.0)

3
4 Lei Ma¹, George Hurtt¹, Lesley Ott², Ritvik Sahajpal¹, Justin Fisk³, Rachel Lamb¹, Hao Tang^{1,7},
5 Steve Flanagan⁴, Louise Chini¹, Abhishek Chatterjee^{2,5}, Joseph Sullivan⁶

6 ¹ Department of Geographical Sciences, University of Maryland, College Park, MD 20770, USA

7 ² Global Modeling and Assimilation Office, NASA Goddard Space Flight Center, Greenbelt, MD 20771, USA

8 ³ Regrow Agriculture Inc., Durham, NH 03824, USA

9 ⁴ Wildland Fire Science, Tall Timbers Research Station and Land Conservancy, Tallahassee, FL 32312, USA

10 ⁵ Universities Space Research Association, Columbia, MD 21046, USA

11 ⁶ Department of Plant Science & Landscape Architecture, University of Maryland, College Park, MD 20770, USA

12 ⁷ Department of Geography, National University of Singapore, 117570, Singapore

13
14 *Correspondence to:* Lei Ma (lma6@umd.edu)

15 16 **Abstract.**

17 Terrestrial ecosystems play a critical role in the global carbon cycle but have highly uncertain future dynamics.
18 Ecosystem modelling that includes the scaling-up of underlying mechanistic ecological processes has the potential
19 to improve the accuracy of future projections, while retaining key process-level detail. Over the past two decades,
20 multiple modelling advances have been made to meet this challenge, including the Ecosystem Demography (ED)
21 model and its derivatives including ED2 and FATES. Here, we present the global evaluation of the Ecosystem
22 Demography model (ED v3.0), which like its predecessors features the formal scaling of physiological processes of
23 individual-based vegetation dynamics to ecosystem scales, together with integrated submodules of soil
24 biogeochemistry and soil hydrology, while retaining explicit tracking of vegetation 3-D structure. This new [model](#)
25 version builds on previous versions and provides the first global calibration and evaluation, global tracking of the
26 effects of climate and land-use change on vegetation 3-D structure, ~~new~~ spin-up process and input datasets, as well
27 as numerous other advances. Model evaluation was performed with respect to a set of important benchmarking
28 datasets, and model estimates were within observational constraints for multiple key variables including: (i) global
29 patterns of dominant plant functional types (broadleaf vs evergreen); (ii) spatial distribution, seasonal cycle, and
30 interannual trends of global Gross Primary Production (GPP); (iii) global interannual variability of Net Biome
31 Production (NBP); and (iv) global patterns of vertical structure including leaf area and canopy height. With this
32 global model version, it is now possible to simulate vegetation dynamics from local to global scales and from

33 seconds to centuries, with a consistent mechanistic modelling framework amendable to data from multiple
34 traditional and new remote sensing sources, including lidar.

35 **1 Introduction**

36 Terrestrial ecosystems and the associated carbon cycle are of critical importance in providing ecosystem services
37 and regulating global climate. Plants store approximately 450-650 Pg C as biomass globally. They remove
38 approximately 120 Pg C from the atmosphere each year through photosynthesis, and release a similar magnitude of
39 carbon to the atmosphere through respiration (Beer et al., 2010; Ciais et al., 2014a). Human activities over past
40 centuries have significantly impacted terrestrial ecosystems through biophysical and biogeochemical mechanisms
41 (Cramer et al., 2001; Walther et al., 2002; Brovkin et al., 2004; Pielke Sr. et al., 2011). Quantification, attribution
42 and future projections of the terrestrial carbon sink requires in-depth understanding of underlying ecological
43 processes and their sophisticated responses and feedbacks to climate change, elevated CO₂, and land use and land
44 cover change (LULCC) across multiple biomes and spatial and temporal scales (Canadell et al., 2007; Erb et al.,
45 2013; Keenan and Williams, 2018). This demand for information has driven the emergence and development of
46 dynamic global ecosystem models (DGVMs), which simplify the structure and functioning of global vegetation into
47 several plant functional types and simulate vegetation distribution and associated biogeochemical and hydrological
48 cycles with ecophysiological principles (Prentice et al., 2007; Prentice and Cowling, 2013). The first generation of
49 DGVMs have been used successfully to address a variety of carbon cycle related questions and integrated into Earth
50 System Models (ESMs) (Cramer et al., 2001; Sitch et al., 2008). Subsequent developments have improved the
51 representation of vegetation demographic processes within ESMs, including the Ecosystem Demography model
52 (ED) (Hurtt et al., 1998; Moorcroft et al., 2001), ED2 (Medvigy 2006; Medvigy et al., 2009; Longo et al., 2019a),
53 CLM(ED) (Fisher et al., 2015; Lawrence et al., 2019; Massoud et al., 2019), SEIB-~~DFVM~~-DGVM (Spatially-
54 Explicit Individual-based Dynamic Global Vegetation Model) (Sato et al., 2007), LPJ-GUESS (Lund-Postdam-Jena
55 General Ecosystem Simulator) (Smith et al., 2001, 2014), and GFDL-LM3-PPA (Geophysical Fluid Dynamics
56 Laboratory Land Model 3 with the Perfect Plasticity Approximation) (Weng et al., 2015), as summarized in Fisher
57 et al., 2018).

58
59 In addition to model development, model evaluation is an important ~~process to for~~ assessing model uncertainties and
60 ~~also identifying~~ processes that need particular improvements (Anav et al., 2013; Luo et al., 2012; Eyring et al.,
61 2019). Considerable effort has been spent on standardizing evaluation practices and developing a comprehensive
62 benchmarking system (Abramowitz et al., 2012; Collier et al., 2018; Eyring et al., 2016; ~~Kelly et al., 2013;~~
63 Randerson et al., 2009). For example, a benchmarking system from the International Land Model Benchmarking
64 (ILAMB) project has been increasingly used to evaluate ecosystem and climate models (Collier et al., 2018;
65 Ghimire et al., 2016; Luo et al., 2012). In parallel, new observations are providing new opportunities to initialize and
66 test models. Of particular relevance for ecosystem models is the advent of spaceborne lidar missions (i.e., GEDI and
67 ICESat-2) (Dubayah et al., 2020a; Markus et al., 2017), which provide unprecedented global observations of forest

68 structure, including vertical distribution of leaf foliage. Building on this past work, and utilizing new observations,
69 an updated and systematic evaluation of model performance ~~on~~[across](#) multiple variables is now possible.

70
71 Here, we present the global evaluation of Ecosystem Demography v3.0. The ED model was developed two decades
72 ago using a formal scaling approach (Size- and Age-Structured approximation, SAS) to efficiently approximate the
73 expected dynamics of individual based forest dynamics (Hurt et al., 1998; Moorcroft et al., 2001). Since its
74 emergence, the ED model has been continuously developed and applied at various regions and spatial scales, with
75 land-use changes, and lidar observations (Hurt et al., 2002, 2004). In the original paper, the model was implemented
76 at [the](#) site scale and primarily evaluated for aboveground biomass accumulation during succession using
77 chronosequence field data, and at the regional scale using 1-degree resolution data on potential biomass, soil carbon
78 and net primary productivity (NPP) (Moorcroft et al., 2001). Most recently, ED was implemented at high spatial
79 resolution (90 m) over a regional domain of the Northeastern United States and evaluated for aboveground biomass
80 using wall-to-wall lidar-based estimates of contemporary biomass at that spatial resolution (Hurt et al., 2019a; Ma
81 et al., 2021). The evaluation included >30 million grid cell pairs, and >10³ forest inventory [field](#) plots. This
82 progression [of development spans includes](#) a range of model capabilities, spatial resolutions, and evaluation data,
83 ~~ranging spanning~~ from coarse resolution potential vegetation, to high spatial resolution contemporary conditions at
84 regional scales. However, development and evaluation of ED at [the](#) global scale for contemporary conditions has not
85 yet been accomplished. In this study, ED v3.0 is evaluated at global scales for the first time. Multiple key variables
86 are considered in the evaluation, including benchmark datasets on vegetation distribution, vegetation structure, and
87 carbon and water fluxes.

88 **2 Methods**

89 ED v3.0 is built upon a series of previous model developments (Moorcroft et al., 2001; Hurt et al., 2002; Albani et
90 al., 2006; Fisk, 2015; Flanagan et al., 2019). To extend ED's capabilities globally, several additional modifications
91 were introduced to capture global vegetation distribution across biomes and related carbon stocks and fluxes. Below,
92 a summary of the ED approach and recent modifications is provided. The full descriptions of each submodule can be
93 found in the Supplement along with tables of parameter values. To conduct the model evaluation, a model
94 experimental protocol including equilibrium and transient simulations was developed and relevant forcing data were
95 identified from global existing datasets. Model simulations were then compared to benchmarking datasets.

96 **2.1 Model**

97 The ED model is an individual based prognostic ecosystem model (Moorcroft et al., 2001). By integrating
98 submodules of growth, mortality, hydrology, carbon cycle, and soil biogeochemistry, ED can track plant dynamics
99 including growth, mortality, and reproduction. Along with plant dynamics, ED can track the carbon cycle, including
100 carbon uptake by leaf photosynthesis, carbon allocation to biomass growth in leaves, roots and stems, carbon
101 redistribution from plants to soil based on plant tissue turnover from dead plants due to mortality and disturbance,

102 carbon decomposition in various pools (metabolic litter pool, structural litter pool, soil slow pool, soil passive pool,
103 wood product pool, harvested crop pool, etc) as well as carbon combustion from fire (Fig. 1 and Fig. 2). Over the
104 last two decades, ED has been continuously developed and combined with lidar and land-use change data to predict
105 ecosystem dynamics and associated water and carbon fluxes across spatial scales (e.g., site to regional and
106 continental) and temporal scales (e.g., short-term seasonal to long-term decadal and century) (Hurt et al., 2002,
107 2004, 2010, 2016, Fisk et al., 2013, Flanagan et al., 2019). ED distinguishes itself from most other ecosystem
108 models by explicitly tracking vegetation structure and scaling fine-scale physiological processes to large scale
109 ecosystem dynamics (Hurt et al., 1998, Moorcroft et al., 2001, Fisher et al., 2018). In ED, vegetation structure (e.g.,
110 height and diameter at breast height), and physiological processes (e.g., leaf photosynthesis and phenology) are
111 modelled at the individual scale, where individual plants compete mechanically for light, water, and nutrients.
112 During implementation, this horizontal heterogeneity is tracked through cohort and patch demography. Explicitly
113 modelling vegetation height facilitates a potential connection to lidar data. ~~The most advanced version of ED was
114 used in this study and it has been recently calibrated and evaluated globally by various benchmarking datasets such
115 as gross primary productivity (GPP), leaf area index (LAI), aboveground biomass (AGB), and net biome
116 productivity (NBP) (Ma et al., 2021).~~

117 2.1.1 Additional modifications

118 Major modifications in ED v3.0 focus on four areas: plant functional type representation, leaf level physiology,
119 hydrology, and wood products. These areas ~~have been found to behave~~ have been identified as particularly important ~~to~~
120 for improving model performance globally.

121
122 Plant functional types describe the characteristics of vegetation in different representative groups for modelling. In
123 previous ED versions, various PFT combinations were implemented to represent vegetation in the respective regions
124 where the model was implemented. In the original implementation of ED for Central and South America, four PFTs
125 were represented (i.e., Early-successional broadleaf, Middle-successional broadleaf, Late-successional broadleaf and
126 C4 grasses (Moorcroft et al., 2001). In a subsequent implementation over North America, two additional PFTs (i.e.,
127 Northern pines and Southern pines) were proposed in Albani et al., 2006. Here, these PFTs are included and further
128 refined as seven major PFTs: ~~namely~~ early-successional broadleaf trees (EaSBT), middle-successional broadleaf
129 trees (MiSBT), late-successional broadleaf trees (LaSBT), northern and southern pines (NSP), late-successional
130 conifers (LaSC), C3 shrubs and grasses (C3ShG), and C4 shrubs and grasses (C4ShG) (Supplement S1). The
131 broadleaf PFTs (i.e., EaSBT, MiSBT, and LaSBT) are distinguished between tropical and non-tropical subtypes.
132 These PFTs primarily differ in their phenology, leaf physiological traits, allometry, mortality rate, and dispersal
133 distance. As in previous versions of ED, the spatial distribution of PFTs is mechanistically determined by individual
134 competition for light, water and nutrients. No quasi-equilibrium climate–vegetation relationships, or other
135 assumptions or observations, are used to constrain the presence or absence of PFTs.

136

137 Leaf physiology determines short-term (i.e., < hourly) leaf-level carbon and water exchanges in response to
138 environmental conditions (air temperature, shortwave radiation, air humidity, wind speed, [and](#) CO₂ level). The
139 representation of leaf level physiology in previous versions of ED (Moorcroft et al., 2001) was taken from IBIS
140 (Foley et al., 1998), which in turn was based on prior work from Farquhar, Collatz, Ball and Berry and others
141 (Farquhar and Sharkey 1982; Ball et al., 1987; Collatz et al., 1991, 1992). Here, ED's representation of leaf level
142 physiology is reformulated for C3 and C4 pathways (Farquhar et al., 1980; Von Caemmerer and Furbank, 1999)
143 with added boundary layer conductance for diffusing water vapor and CO₂ between ambient air and leaf surface, and
144 parameterized with temperature dependence functions from other studies (Bernacchi et al., 2001; von Caemmerer et
145 al., 2009; Kattge and Knorr, 2007; Massad et al., 2007; Von Caemmerer, 2000, Supplement S3).

146
147 Hydrology controls the water available for vegetation. The hydrology submodule in ED tracks soil moisture
148 dynamics between incoming water flow from precipitation and outgoing flow through percolation, runoff, and
149 transpiration. Previous ED versions did not include evaporation from soil and canopy and also did not account for
150 snow dynamics. Here, evaporation from soil and canopy is estimated based on the Penman-Monteith (P-M) equation
151 (Monteith, 1965; Mu et al., 2011). In addition, a simple snow dynamics process is introduced to decrease water
152 availability for plants when air temperature drops below the freezing point and increase it when air temperature rises
153 above freezing point at a rate depending on air temperature. More details can be found in Supplement S9.

154
155 Land use activities (e.g., deforestation and wood harvesting) remove vegetation carbon from ecosystems for various
156 purposes. This carbon is traditionally tracked in wood product pools, with different lifetimes and temporal emissions
157 to the atmosphere. The previous land use submodule in ED only tracked changes in vegetation and soil carbon
158 during various land use activities but did not track subsequent decay process of product pools (Hurt et al., 2002). In
159 ED v3.0, three wood product pools are added to track the life cycles of harvested wood and associated decay
160 processes (Supplement S11). Wood product pools gain carbon from land use activities such as wood harvesting or
161 deforestation, and lose carbon through decay and emissions to the atmosphere. The loading of these product pools,
162 and their decay rates, are based on a prior study (Hansis et al., 2015).

163 **2.2 Model initialization [and overview of experiments](#)**

164 Global spin-up of ED initialized ecosystems to contemporary conditions by taking into account climate change,
165 rising CO₂, and land use change. The global spin-up was comprised of two separate runs at 0.5° spatial resolution.
166 The first run, called the “equilibrium simulation”, ran ED from initial conditions to equilibrium. This run was
167 performed for 1000 years by which time PFT composition and carbon pools of vegetation and soil reached a
168 dynamic equilibrium. The second run, called “transient simulation”, restarted from the end of the equilibrium
169 simulation and simulated for 1166 years, corresponding to the period A.D. 851 – A.D. 2016, with varying CO₂
170 levels, land-use change, and climate variability. Both runs were driven with meteorological forcing from NASA
171 Modern-Era Retrospective analysis for Research and Applications, version 2 (MERRA2) (Gelaro et al., 2017) and
172 surface CO₂ concentration from NOAA CarbonTracker Database, version 2016 (NOAA CT2016) (Peters et al.,

173 2007, with updates documented at <http://carbontracker.noaa.gov>). Additionally, the transient simulation run utilized
174 prescribed burned area from the Global Fire Emissions Database, version 4 (GFED4) (Randerson et al., 2015) and
175 forced land-use change from Land Use Harmonization, version 2 (LUH2) (Hurtt et al., 2019b, 2020). Details of
176 these simulations are provided below.

177

178 The equilibrium simulation was started from bare ground where the soil and vegetation carbon pools were set at
179 zero, and all PFTs were initialized with equal seedling density for all patches and all grid cells over the globe. This
180 run was driven for 1000 years with MERRA2 climatology of 1981-1990 and NOAA CT2016 average surface CO₂
181 between 2001-2014 (with spatial variation and global average rescaled to 280 ppm). No climatic envelope or
182 potential biome maps were used to constrain PFT spatial distribution; competition determined final PFT
183 distributions, vegetation structure, and carbon stocks. The land-use change module was disabled in this run of
184 simulation.

185

186 The transient simulation was restarted from equilibrium conditions. The land-use change submodule was activated,
187 and all land-use transition types from LUH2 were incorporated into the simulation at annual time steps. These
188 transitions included changes in agriculture and forest extent, shifting cultivation, and wood harvesting, among
189 others. MERRA2, NOAA CT2016 and GFED were used throughout the simulation with varying temporal settings
190 depending on data availability. Specifically, for MERRA2, a climatology between 1981-1990 was used until 1981,
191 and annual meteorology was used subsequently. For NOAA CT2016, an average surface CO₂ concentration between
192 2001-2014, which varies spatially and grows over time, was used until 2000, while annual NOAA CT2016 surface
193 CO₂ concentrations were used subsequently. For GFED4 burned area, an average between 1996-2016 was used until
194 1996, after which annual burned area was used.

195 **2.3 Forcing data**

196 Meteorological variables utilized from MERRA2 include surface air temperature (TLML), surface specific humidity
197 (QLML), precipitation (PRECTOTCORR), incident shortwave radiation (SWGDN), surface wind speed (SPEED),
198 and multi-layer soil temperature (TSOIL1-TSOIL3). Original estimates of surface air temperature, surface specific
199 humidity, incident shortwave radiation, and surface wind speed were averaged from daily hourly to monthly hourly
200 for each year between 1981 to 2016. The resulting annual monthly average of diurnal meteorological variables were
201 used to drive the leaf physiology submodule in ED. Hourly surface air temperature, precipitation, and soil
202 temperature were also aggregated to monthly averages for each year between 1981 to 2016, and then used to drive
203 the soil hydrology, phenology, evapotranspiration, and biogeochemical modules in ED.

204

205 Surface CO₂ concentration was extracted from the lowest vertical level of NOAA CT2016 CO₂ mole fraction which
206 is temporally and spatially varying. The original datasets were first linearly interpolated from 3°x2° (longitude x
207 latitude) to 0.5°x0.5° and from 3-hour to hourly, and then averaged to monthly hourly estimates for each grid cell
208 and each year between 2001 and 2014, resulting in surface CO₂ concentration maps with 4032 timesteps (14 years,

209 24 hours, 12 months) for each 0.5°x0.5° grid. The surface CO₂ concentration maps were used to drive the transient
210 simulation from 850 to 2000, retaining average spatial variation between 2001 and 2014 and applying a scaling
211 factor to force the global annual average CO₂ concentration to remain at 280 ppm before 1850, then grow linearly to
212 310 ppm in 1950 and to 375 ppm in 2000. This increasing trend in global average matches observed CO₂ growth
213 rates from Keeling (2008).

214
215 LUC forcing was derived from the LUH2 (version v2h) for years 850-2015 (Hurtt et al., 2019b, 2020). The original
216 land use state and land use transitions were aggregated from a spatial resolution of 0.25°x0.25° to 0.5°x0.5° for each
217 year between 850 and 2015. Subtypes of land use states and associated transitions were grouped into the major land
218 use types of the model's predecessor version (LUH1). Specifically, sub crop types of C3 annual crops (c3ann), C3
219 perennial crops (c3per), C4 annual crops (c4ann), C4 perennial crops (c4per) and C3 nitrogen-fixing crops (c3nfx)
220 were all merged as cropland. Forested primary land (primf) and non-forested primary land (primn) were merged as
221 primary land; forested secondary land (secdf) and non-forested secondary land were merged as secondary land; and
222 managed pasture (pastr) and rangeland were merged as pasture. Note that all types of land use transitions and gross
223 transition rate were used in ED's land use module.

224
225 Soil properties, including depth, hydraulic conductivity, and residual and saturated volumetric water content are
226 important for determining plant water availability. These soil properties were taken from Montzka et al. 2017.
227 Additional details can be found in the supplement (S9, hydrology submodule).

228 **2.4 Model evaluation**

229 A benchmarking package of data (Table 1) was collected to evaluate ED performance. Eight critical variables,
230 [proven to be important for terrestrial biogeochemical cycles \(Spafford and MacDougall 2021\)](#), were assessed in
231 four categories including: PFT distribution, carbon stocks in vegetation and soil, carbon and water fluxes, and
232 vegetation structures in terms of canopy height and vertical LAI. Evaluation was carried out at different spatial (grid,
233 latitudinal, and biome) and temporal scales (climatological, seasonal, and interannual). For each variable, a widely
234 used dataset was used for reference, and in some cases, these span different years. An important feature of our
235 method was to adjust the simulation years from ED to match each benchmarking dataset.

236 **2.4.1 Vegetation distribution**

237 The satellite-based land cover product, ESA CCI, was used to examine the distribution of three modelled PFTs,
238 grass, broadleaf trees, and needleleaf trees (ESA 2017). Many satellite-based land cover datasets differ largely from
239 ED in PFT definition. For example, no successional PFTs exist in ESA CCI land cover types. Thus, the native PFTs
240 in ED and ESA CCI both have to be aggregated to broader categories such as broadleaf PFTs, needleleaf PFTs, and
241 grass PFTs. To do this, the 22 native land cover classes of ESA CCI were first reclassified to 'broadleaf evergreen
242 tree', 'broadleaf deciduous tree', 'needleleaf evergreen tree', 'needleleaf deciduous tree', 'natural grass' and
243 'manned grass' using a cross-walk table (Poulter et al., 2015). They were then further merged by phenology type

244 and aggregated to 0.5°, resulting in PFT fraction maps of broadleaf PFTs, needleleaf PFTs, and grass and shrub
245 PFTs. ED PFTs of EaSBT, MiSBT and LaSBT were merged as broadleaf PFTs, NSP and LaSC were merged as
246 needleleaf PFTs, and C3ShG and C4ShG were merged as grass and shrub PFTs.

247 **2.4.2 Carbon fluxes**

248 Evaluation of carbon fluxes focused on Gross Primary P-Production (GPP) and Net Biome P-Production (NBP).
249 Modelled GPP was evaluated with respect to spatial pattern, seasonality, and interannual variability using two
250 satellite data-driven GPP datasets, FLUXCOM (Jung et al., 2020) and FluxSat (Joiner et al., 2018), and the satellite-
251 retrieved sun-induced chlorophyll fluorescence (CSIF) dataset (Zhang et al., 2018). The FLUXCOM and FluxSat
252 datasets are derived from a data-driven approach that combines carbon fluxes measurements from FLUXNET and
253 satellite observations from MODIS. Major differences between FLUXCOM and FluxSat include the use of
254 meteorological forcing and the specific approach used. FLUXCOM used meteorological forcing and a machine
255 learning approach, while FluxSat used a simplified light-use efficiency model that does not rely upon meteorological
256 forcing. FluxSat also used satellite-based sun-induced chlorophyll fluorescence (SIF) to delineate highly productive
257 regions. Satellite measurements of SIF have recently been suggested as a promising proxy of terrestrial GPP,
258 exhibiting high sensitivity to plant photosynthetic activities (Lee et al., 2013; Guanter et al., 2014; Yang et al.,
259 2015). In this study, we chose the CSIF dataset for its improved spatiotemporal continuity. CSIF is generated by
260 fusing Orbiting Carbon Observatory-2 (OCO-2)-retrieved SIF and MODIS reflectance data using a machine learning
261 approach. FLUXCOM, FluxSat, and CSIF were all resampled to monthly estimates at 0.5x0.5 spatial resolution
262 before the evaluation.

263
264 Modelled net biome productivity (NBP) was compared against multiple sources including estimates from process-
265 based models, atmospheric inversions, and the 2020 global carbon budget (GCB2020) (Friedlingstein et al., 2020).
266 For process-based models, 17 DGVMs reported in the GCB2020 were used to calculate the respective net land sink
267 by differencing land uptake and land use emissions estimates (i.e., $S_{LAND} - ELUC$). For atmospheric inversions, three
268 systems are used, namely CarbonTracker Europe (CTE) (van der Laan-Luijkx et al., 2017), Jena CarboScope
269 (version s81oc) (Rödenbeck et al., 2008) and the Copernicus Atmosphere Monitoring Service (CAMS) (Chevallier
270 et al., 2005). The three inversions all derive surface carbon fluxes using atmospheric CO₂ measurements, prior
271 constraints on fluxes, and an uncertainty and atmospheric transport model, but vary with respect to the specific data,
272 prior constraints, and transport models used (Peylin et al., 2013). In the GCB2020, the residual terrestrial sink was
273 used, which was calculated as total emissions from fossil fuel and land use change minus the atmospheric CO₂
274 growth rate and ocean sink (i.e., $E_{FF} + ELUC - G_{ATM} - S_{OCEAN}$).

275 **2.4.3 Carbon stocks**

276 Modelled carbon pools were evaluated with regards to vegetation aboveground biomass (AGB) and soil carbon. The
277 reference AGB data included estimates from Santoro et al. (2018) and Spawn et al. (2020). These two AGB datasets
278 provide high spatial resolution (e.g., 100 m to 1000 m) wall-to-wall global estimates of the year 2010, but differ in

279 their methodologies. Specifically, AGB from Santoro et al. (2018) was produced by combining spaceborne synthetic
280 aperture radar (SAR) (ALOS PLASAR, Envisat ASAR), Landsat-7, and Lidar observations from Ice, Cloud, and
281 land Elevation Satellite (ICESat). AGB from Spawn et al. (2020) includes biomass of forests and also other woody
282 non-forest plants. Reference soil carbon was from the Harmonized World Soil Database (HWSD) (Wieder et al.,
283 2014), including soil carbon for topsoil (0 to 30 cm) and subsoil (30 to 100 cm).

284 2.4.4 Water fluxes

285 Modeled ET was evaluated against the FLUXCOM dataset (Jung et al., 2019) which used meteorological forcing,
286 remote sensing data, and a machine learning approach to scale up the measurements from FLUXNET eddy
287 covariance towers to the global scale. This dataset provides gridded estimates at resolution of 0.0833° for the period
288 of 1981-2014. The FLUXCOM dataset was resampled to monthly estimates at 0.5x0.5 spatial resolution before
289 evaluation.

290 2.4.4.5 Vegetation structure

291 Evaluation of modelled forest structure focused on total and vertical distribution of leaf area index (LAI) and tree
292 canopy height. Two reference LAI products, namely MODIS MCD15A3H (Myneni et al., 2015) and GEOV2 LAI
293 (Verger et al., 2014), ~~are~~ were used for evaluating total LAI in terms of spatial distribution, seasonality, and
294 interannual variability. The MODIS and GEOV2 LAI datasets were both derived from passive optical observations
295 with empirical-based inversion methods which relate leaf area with optical canopy reflectance or vegetation indices;
296 however, these two products vary with source of optical observations and choices for inversion methods. Reference
297 vertical LAI was from the Global Ecosystem Dynamics Investigation (GEDI) L2B products, which retrieves leaf
298 vertical distribution from lidar waveform return (Dubayah et al., 2020b). Reference canopy height data were based
299 on direct forest structure observations from GEDI L2A (Dubayah et al., 2020c) and the ICESat-2 ATL08 products
300 (Neuenschwander et al., 2020). Mean canopy height was generated at 0.5° spatial resolution from the relative height
301 98th percentile (RH98) of all GEDI L2A footprints and canopy top height (h_canopy) ~~of~~ and all ICESat-2 ATL08
302 segments of good quality.

303 **3 Results**

304 ED results were evaluated across four primary categories: PFT distribution, vegetation and soil carbon pools, carbon
305 and water fluxes, and vegetation structure. Evaluation included comparing modelled global quantities, and their
306 associated spatial and temporal patterns, to the benchmarking datasets.

307 **3.1 Evaluation of PFT distribution**

308 Global total area of broadleaf PFTs, needleleaf PFTs and grass and shrub PFTs were estimated by ED to be 24.30,
309 8.93 and 24.63 million km², respectively. These results compare to ESA CCI data which estimate the same
310 respective global PFT areas at 20.13, 10.65 and 41.49 million km². The global spatial distribution and corresponding

311 zonal distribution of broadleaf PFTs, needleleaf PFTs and grass and shrub PFTs are shown in Fig. 3. In this
312 comparison, the major patterns of ED estimated PFT distribution were similar to the observed distribution of PFTs.
313 ED estimated needleleaf PFTs were dominate at high latitudes, broadleaf PFTs dominated in the tropics, and grass
314 and shrub PFTs were widespread globally. ED also predicted the observed coexistence of broadleaf and needleleaf
315 PFTs in southern China and eastern US. However, beyond these major patterns, ED estimates differed in some
316 specific regions. For example, ED predicted the existence of needleleaf PFTs along the Andes Mountains in South
317 America and in southern Australia. While this pattern was not evident in the ESA CCI data, there are other studies
318 based on ground observations that support it (Farjon and Filer, 2013). ED also estimated relatively more broadleaf
319 PFTs in eastern Europe and southern China, ~~less-fewer~~ broadleaf PFTs in Africa savanna, less needleleaf PFTs in
320 east Siberia, and less grass and shrub PFTs both in Africa savanna and northern China. Analogous results can also
321 be seen zonally, where major patterns of PFTs are broadly similar to observed but with some specific differences. In
322 terms of zonal distribution per PFT, the smallest discrepancies between ED and ESA CCI appear in broadleaf PFTs,
323 followed by needleleaf PFTs, and grass and shrub PFTs. [Spatial distribution maps for each of seven PFTs from ED](#)
324 [can be found in Fig. S1.](#)

325 3.2 Evaluation of AGB and soil carbon

326 ED estimates of AGB were compared to corresponding benchmark data. ED estimated global total aboveground
327 vegetation carbon (including forest and non-forest) at 298 Pg C in 2010. This compares to 283 Pg C and 297 Pg C
328 estimated by Spawn et al. (2020) and Santoro et al. (2018). ED's estimate of the spatial pattern of AGB was also
329 comparable to that of both ~~two~~ benchmark datasets, with the highest biomass densities [found](#) across the tropics (i.e.,
330 the Amazon rainforest, the Congo river basin, and southeast Asia) with declining biomass densities northward
331 towards the temperate and boreal regions. For example, similar to observations, average estimated AGB density was
332 $\sim 15 \text{ kg C/m}^2$ in the tropics and less than 2.5 kg C/m^2 across temperate and boreal regions (Fig. 4d). In addition, the
333 AGB transition along the African forests-savanna zone was represented by ED, albeit with lower values in the
334 savanna. Major discrepancies between ED and benchmarking data appear in southern China, southeast Asia and
335 southeast Brazil.

336
337 ED estimates of soil carbon were compared to benchmark data on soil carbon. ED estimated total global soil carbon
338 at 671 Pg C in 2000, which was within the range of CMIP5 ESMs (510 - 3040 Pg C) (Todd-Brown et al., 2013), but
339 lower than the HWSD estimate of 1201 Pg C. Comparing total stocks at the biome level (Fig. 5d) showed that ED
340 generally reproduced soil carbon variation across biomes, but notably underestimated carbon in boreal forest/taiga,
341 deserts and xeric shrublands, tropical and subtropical grasslands, savannas and shrubland. The soil carbon map from
342 ED revealed different spatial patterns compared to HWSD, with relatively less spatial heterogeneity and fewer
343 regions with densities above 30 kg C/m^2 .

344 3.3 Evaluation of GPP, NBP and ET

345 Globally, the ED estimate of average annual GPP was 134 Pg C yr⁻¹ between 2001-2016, which compares to 120 Pg
346 C yr⁻¹ from FLUXCOM and 136 Pg C yr⁻¹ from FluxSat over the same period. The spatial pattern of GPP from ED
347 was also compared to benchmark values at the grid and latitudinal scales (Fig. 6). Similar to observations, areas of
348 highest productivity occur in the tropics, followed by [the](#) temperate and boreal regions. For the tropics, ED was ~0.5
349 kg C/m²/yr higher than FLUXCOM, and ~0.2 kg/C/m² higher than FluxSat, but lower than both over the Africa
350 Savanna. Additionally, ED was relatively higher in southern China and Brazil than either benchmark dataset. A
351 notably increasing annual trend in total global GPP can be seen in both ED and FluxSat estimates between 2001-
352 2016 as well as from globally averaged CSIF (Fig. 7). ED also reproduced GPP interannual variability from FluxSat,
353 FLUXCOM and CSIF, dipping in the years 2005, 2012 and 2015; and peaking in 2006, 2011 and 2014. Regarding
354 latitudinal seasonality at the biome scale (Fig. 8), ED captured GPP timing for most latitudinal zones, including 60°
355 - 90°N, 45° - 60°N, 15° - 30°N and 60° - 30°S. Major differences appear in 30° - 45°N, where ED shows [a decreases](#)
356 from July-September, and in 15°S - 0°, where ED shows delayed monthly timing of lowest annual GPP values.

357
358 Globally, the ED estimate of average annual NBP between 1981 and 2016 was 1.99 Pg C/yr, which can be
359 compared to 1.21-1.80 Pg C/yr from atmospheric inversions, 1.11 Pg C/yr from DGVMs, and 1.31 Pg C/yr from [the](#)
360 GCB2020 residual terrestrial sink. ED estimates were also compared to benchmark datasets on global changes over
361 time (Fig. 9). Similar to the references, ED estimated an increasing trend with substantial interannual variation
362 during the 1981-2015 period. This variation included reductions in El Niño years (such as 1983, 1998 and 2015) and
363 increases in La Niña years (such as 1989, 2001-2002 and 2011). An exception is 1991-1992, where ED and DGVMs
364 were both lower than atmospheric inversions. This period includes the Mt. Pinatubo eruption, [the](#) effect of which is
365 not included in the shortwave radiation forcing of GCB2020 DGVMs or ED (Mercado et al., 2009; Friedlingstein et
366 al., 2020). During the period 2007-2016, ED produced a continued increasing trend [over the 2007-2016 period](#) as
367 reflected in the mean of atmospheric inversions, but not the mean of DGVMs. Specifically, ED estimated NBP
368 averaged 2.34 Pg C/yr from 2007-2016, which as within the range of the atmospheric inversions estimates (1.77 -
369 2.64 Pg C/yr) and DGVMs estimates (0.58 - 2.82 Pg C/yr), but higher than either the mean of DGVMs (1.40 Pg
370 C/yr) or the GCB2020 residual terrestrial sink (1.81 Pg C/yr). Despite the similarities in global trends, the latitudinal
371 comparison between ED and atmospheric inversions indicated contrasting attribution of the global sink (Fig. 10). In
372 comparison to the atmospheric inversions, ED predicted a stronger sink in tropics and relatively weaker sink in the
373 Northern Hemisphere. Such a pattern was highlighted in the global carbon budget (Friedlingstein et al., 2020),
374 where process-based models and the atmospheric inversions generally show less agreement on the spatial pattern of
375 the carbon sink in these two regions. There is recognized uncertainty about the underlying actual pattern due in part
376 to the in-situ network, which is spatially biased towards the mid-latitudes (i.e., more observational sites) relative to
377 the tropics (i.e., fewer observational sites) (Ciais et al., 2014b).

378
379 Globally, the ED estimate of global mean annual ET between 1981 and 2014 was 393.46 mm/yr, which can be
380 compared to 582.10 mm/yr from FLUXCOM. ED estimates of ET were also compared to gridded FLUXCOM data

381 and by latitude (Fig. 11). Similar to the reference dataset, ED estimated the highest rates across the tropics with
382 decreases towards high latitudes. This pattern generally followed the spatial distribution of precipitation. ED estimates
383 were close to FLUXCOM over the tropics (i.e., 1500 mm/yr) as well as latitudes above 60°N and below 35°S (i.e.,
384 below 500 mm/yr), but notably underestimated average annual ET in other latitudes. ED estimates were generally
385 smaller than FLUXCOM in dry regions such as southern Africa and interior Australia.

386 3.4 Evaluation of canopy height and LAI vertical profile

387 Evaluation of vegetation structure estimates focused on leaf area and canopy height. Fig. 12 presents the spatial
388 distribution of growing season LAI from ED, GEOV2, and MODIS. Growing season LAI is chosen for comparison
389 because winter snow in the northern region (e.g., boreal forests) might affect LAI retrieval and cause uncertainties in
390 remote sensing estimates (Murray-Tortarolo et al., 2013). There was good agreement in spatial pattern between ED
391 and reference LAIs (Fig. 12d), showing peaks in the tropics and boreal region (near 50°N), and relatively low
392 estimates across temperate regions. In the tropics, ED estimated an average LAI of 6.0 m²/m², which was similar to
393 GEOV2 but higher than MODIS. However, ED produced higher LAI in temperate and boreal regions than both
394 reference datasets, specifically in southern China and Brazil. Despite these differences there was a general
395 agreement in the greening trend between 1999 and 2016 (as shown in Fig. 13). The linear fitted LAI trend was 0.058
396 m²/m² per decade for ED, 0.090 m²/m² for GEOV2, and 0.046 m²/m² for MODIS. LAI seasonality was also
397 compared across latitudinal bands in Fig. 14. Similar to references, ED captured peak season in latitudinal bands 60°
398 - 90°N, 45° - 60°N, and 60° - 30°S, but shows less agreement with the references in the tropics (0° - 15°N and 15S°
399 - 0°). In addition, ED LAI in winter is larger than either reference LAI; at latitudes above 45°N, and between 30°N
400 and 45°N, ED LAI is higher for all seasons. Similarly, higher LAI also appears in 60°S - 30°S, across southern
401 China and Brazil.

402
403 The estimated vertical profile of LAI from ED was compared to GEDI both spatially and [by latitude](#)
404 [band/latitudinally](#). Spatially, ED and GEDI L2B had a similar spatial pattern with most vegetated regions having
405 concentrated LAI under 10m, and only tropical forests, part of southern China and the US having substantial LAI
406 above 30m (Fig. 15). Comparisons of LAI profiles by latitude band indicate close agreement in each zone, and with
407 all regions having the highest values of LAI closest to the ground (0-5 m [and 5-10 m](#)) and decreasing with canopy
408 height (Fig. 16). Discrepancies can be seen at the 0--5_m [and 10--15m LAI](#) interval [along at most](#) latitudinal bands
409 [of 30° - 15°S and 45° - 30°S](#), where ED tends to be higher [0-5m, and lower in the 10-15m bin](#).

410
411 Tree canopy height estimates from ED were compared with satellite lidar observations from GEDI and ICESat-2
412 (Fig. 17). Like the reference datasets, ED produced a spatial pattern with taller trees in tropical rainforests, southern
413 China and the eastern US. The canopy height gradient from forests to savannas in South America (northwest to
414 southeast) and in Africa (central to north and south) were also generally captured by ED. Latitudinal comparison
415 shows ED estimated average height is above 30 m in tropics and is ~10m in temperate regions. The general

416 differences between ED and reference datasets are less than 10_m across all latitudes. However, ED tree height in
417 southern China and Brazil was higher than the references, and lower than references across African savanna.

418 **4 Discussion and Conclusions**

419 Previous studies have developed benchmarking packages and designed model intercomparison activities to evaluate
420 model performance (Abramowitz et al., 2012; Collier et al., 2018; Eyring et al., 2016; Ghimire et al., 2016; Kelly et
421 al., 2013; Luo et al., 2012; Randerson et al., 2009; Sitch et al., 2008). Like those studies, we evaluated ED model
422 results using many key datasets and variables. The work here has utilized a particularly wide range of variables,
423 utilized including the latest versions of key forcing data on climate and land-use, and added a new focus on
424 vegetation structure.

425
426 ~~In this study, we developed a new global version of the Ecosystem Demography model and evaluated it against~~
427 ~~benchmark datasets for a wide range of important variables spanning carbon stocks, carbon and water fluxes,~~
428 ~~vegetation distribution, and vegetation structure. Historically, different models have been developed separately in~~
429 ~~areas of biogeochemistry, biogeography, and biophysics, and in some cases important patterns have been set through~~
430 ~~observations or other prior constraints (Bonan, 1994; Dickinson, 1993; Haxeltine and Prentice, 1996; Hurtt et al.,~~
431 ~~1998; Lieth, 1975; Neilson, 1995; Parton, 1996; Potter et al., 1993; Prentice et al., 1992; Raich et al., 1991; Sellers et~~
432 ~~al., 1986). The ability of this model to reliably simulate such a wide range of phenomena globally in a single~~
433 ~~mechanistic and consistent framework represents an important interdisciplinary synthesis, a functional modelling~~
434 ~~advance, and to our knowledge is unprecedented.~~

435 ED v3.0 includes modifications in four major areas (i.e., PFT representation, leaf level physiology, hydrology, and
436 wood products) to improve model performance at the global scale. These modifications have several qualitative
437 benefits. The refinement of PFTs provides a more complete representation of global vegetation functional types
438 spanning from deciduous to evergreen, from broadleaf to needleleaf, from C3 to C4, from softwood to hardwood.
439 Updated temperature dependence functions in the leaf physiology submodule provides improved calibration and
440 validation with independent field studies. The hydrology submodule now includes characterization of evaporation
441 and snow which were missing in previous regional versions. The land-use submodule now includes a wood product
442 pool which facilitates tracking of the magnitude and timing of vegetation carbon loss and emissions due to
443 deforestation and wood harvesting. These modifications also led to improved quantitative performance against a
444 range of important benchmarks.

445
446 ED estimation of carbon stocks and fluxes compared favourably to benchmarking datasets across a range of spatial
447 and temporal scales, from grid cell to global, and from seasonal to decadal. Similar to benchmarking datasets, ED
448 reproduced latitudinal gradients of GPP and AGB, a positive trend in global total GPP, global total AGB and GPP
449 within reference ranges, and interannual variation of NBP in response to El Niño and La Niña events. Producing
450 such patterns of both global carbon fluxes and stocks is challenging, as it requires models to have the ability to
451 mechanistically scaling up physiological processes from the leaf to ecosystem scales. It also requires models to

452 accurately characterize responses of ecosystem demographic processes to climate change, soil conditions, and land
453 use activities. As a part of a new generation of DGVMs attempting to meet these challenges, ED leverages [advances](#)
454 ~~in detailed advances in~~ understanding of ecosystem-physiology (e.g., Ball–Berry stomatal conductance model and
455 Farquhar photosynthesis model) (Ball et al., 1987; Farquhar 1980), soil biogeochemistry (e.g., CENTURY soil
456 model) (Parton 1996), and processes of disturbance and recovery (e.g., LUH1/LUH2 modelling of land-use
457 transition through time) (Hurtt et al., 2011, 2020). ~~This study is the first, to our knowledge, to combine ecosystem~~
458 ~~demography and land use history to simulate global carbon dynamics and compare to a wide range of benchmarks.~~
459

460 In addition to carbon stocks and fluxes, ED simultaneously estimated the spatial distribution of ~~the seven~~ major
461 PFTs globally. ED [reproduced](#) dominance of broadleaf PFT in tropics and needleleaf PFT in high latitudes, which is
462 similar to benchmarking data. The ability to estimate these patterns mechanistically required the ability to
463 characterize functional plant traits and trade-offs of vegetation as well as the processes and timescales of
464 competition for light, water, and other resources. Numerous studies have made previous advances which contributed
465 to the progress in this study. For example, plant traits have been observed and compiled [crossing across](#) a wide range
466 [of](#) species and geographical domains (Reich ~~1997~~ et al., 1997; Kattge et al., 2011, 2020). Individual based/gap
467 models have been developed to track the life cycle of each individual tree and competition between individuals ~~on~~ [at](#)
468 [the](#) plot and site levels (Botkin et al., 1972; Shugart and West 1977; Shugart et al., 2018; Pacala et al., 1996).
469 Meanwhile, the SAS scaling approach was previously developed to efficiently scale up the individual scale to
470 ecosystem dynamics at regional and continental scales (Hurtt et al., 1998; Moorcroft et al., 2001).

471
472 ED estimation of vegetation structure was also evaluated against benchmark data, in this case, novel observations
473 [using from](#) lidar remote sensing [data](#). Impressively, ED mechanistically and independently produced latitudinal
474 mean height and LAI profiles similar to benchmarking datasets on vegetation structure. This progress is perhaps the
475 most novel achievement because progress on this topic was previously limited due to lack of global observations of
476 vegetation structure. Importantly, the ED model is natively height-structured, in that all trees have explicit height.
477 Originally, this feature was included to enable simulation of individual-based competition for light. This feature
478 however also offers the potential for direct connection to lidar observations on vegetation structure for the purpose
479 of model validation and/or initialization. Numerous studies have been completed at local and regional scales by
480 initializing the ED model with airborne lidar data, demonstrating the power of lidar technique in improving
481 characterization of contemporary ecosystems conditions (Hurtt et al., 2004, 2010, 2016, 2019a and Ma et al., 2021).
482 The advent of GEDI (Dubayah et al., 2020a) and ICESat-2 (Markus et al., 2017) has now expanded the potential for
483 model evaluation and initialization to global scales.

484
485 Despite all of these advances, ~~no model is perfect. There there~~ are [several](#) important examples of differences
486 between ED estimates and reference values that present important challenges for the future. ~~Two~~ [Four](#) ~~examples are~~
487 [important to consider further](#). First, ED estimates of AGB/GPP exceeded reference values in some regions, most
488 notably southern China, southeast Asia and southeast Brazil. Correspondingly, ED also tended to overestimate tree

489 height in these same regions. The discrepancies share a similar spatial pattern and are likely interrelated. One
490 hypothesis is that this overestimation may result at least in part from the land-use forcing. ~~The~~LUH2 has been
491 shown to underestimate harvesting area on primary forest in southern China, and Southeast Asia for the period after
492 1950, and also underestimates total cropland area in Brazil (Chini et al., 2021). LUH2 is being continuously updated
493 and improved through ~~the~~its contribution to the Global Carbon Budget project (Chini et al., 2021). Second, while
494 relative patterns for soil carbon showed close agreement at ~~the~~ biome level for the majority of biomes, the absolute
495 magnitude of soil carbon was much lower than reference for several biomes and thus globally. Before over-
496 interpreting these differences, it should be noted that there are substantial uncertainties with current empirical soil
497 carbon maps in terms of both global totals and spatial distribution (Todd-Brown et al., 2013). Model errors in soil
498 carbon may arise from poor representations of biophysical conditions, inaccurate parameterization, or lack of other
499 important drivers. Soil carbon representation in ED, like that of many other DGVMs/ESMs, is highly simplified ~~and~~
500 ~~the relatively low soil carbon is consistent with a relatively short residence time of soil carbon (about 11.4 years),~~
501 ~~which was close to the lower bound of other CMIP6 ESMs (Ito et al., 2020). Third, ED estimates of ET were lower~~
502 ~~than reference across all latitudes. One reason for this difference could be the parameterization of Penman-Monteith~~
503 ~~equations in the Hydrology submodule, as the value of aerodynamic resistance used in this study was higher than~~
504 ~~reported in Mu et al 2011. A second potential cause could be the scaling of evapotranspiration (Bonan et al 2021),~~
505 ~~which combines cohort scale transpiration with patch scale evaporation and currently omits vertical variation of~~
506 ~~evaporation. Finally, the seasonality of GPP and LAI in tropics differed from reference datasets. The pattern and~~
507 ~~timing of seasonality in the tropics is scientifically challenging to understand and has been the subject of several~~
508 ~~recent studies (Morton et al., 2014; Saleska et al., 2016; Tang et al., 2017). In ED, similar to other DGVMs/ESMs,~~
509 ~~soil water availability is assumed as the primary driver of tropical phenology. Such mechanisms lead to reduced LAI~~
510 ~~and GPP over dry seasons, which contrast to observations (Restrepo-Coupe et al., 2016), and strongly driven by~~
511 ~~NPP and soil temperature, but these two drivers have been shown to only explain a small amount of spatial variation~~
512 ~~in the HWSO map (Todd-Brown et al., 2013). The underestimation in the boreal forest/Taiga biome in particular is~~
513 ~~likely due to a combination of these factors. Ongoing research through the NASA Arctic Boreal Vulnerability~~
514 ~~Experiment (ABOVE) program and the Next-Generation Ecosystem Experiments (NGEE Arctic) program will likely~~
515 ~~improve both the data and model parameterization in this critical region.~~

516

517 In this study, we developed a new global version of the Ecosystem Demography model and evaluated it against
518 benchmark datasets for a wide range of important variables spanning carbon stocks, carbon and water fluxes,
519 vegetation distribution, and vegetation structure. Historically, different models have been developed separately in
520 areas of biogeochemistry, biogeography, and biophysics, and in some cases important patterns have been
521 established ~~set~~ through observations or other prior constraints (Bonan, 1994; Dickinson, 1993; Haxeltine and
522 Prentice, 1996; Hurtt et al., 1998; Lieth, 1975; Neilson, 1995; Parton, 1996; Potter et al., 1993; Prentice et al., 1992;
523 Raich et al., 1991; Sellers et al., 1986). The ability of this model to reliably simulate such a wide range of
524 phenomena globally in a single mechanistic and consistent framework represents an important interdisciplinary
525 synthesis, a functional modelling advance, and to our knowledge is unprecedented.

526 ~~Previous studies have developed benchmarking packages and designed model intercomparison activities to evaluate~~
527 ~~model performance (Abramowitz et al., 2012; Collier et al., 2018; Eyring et al., 2016; Ghimire et al., 2016; Kelly et~~
528 ~~al., 2013; Luo et al., 2012; Randerson et al., 2009; Sitch et al., 2008). Like these studies, we evaluated ED model~~
529 ~~results using many key datasets and variables. The work here has utilized a particularly wide range of variables,~~
530 ~~utilized the latest versions of key forcing data on climate and land use, and added a new focus on vegetation~~
531 ~~structure.~~

532
533 Future work will focus on addressing the limitations discussed above and making direct connections with lidar forest
534 structure observations from GEDI and ICESat-2 to improve demographic processes, and the quantification and
535 attribution of the terrestrial carbon cycle. Meanwhile, the global development and evaluation of ED demonstrates the
536 model's ability to characterize essential aspects of terrestrial vegetation dynamics and the carbon cycle for a range of
537 important applications. This model has recently been integrated with NASA's Goddard Earth Observing System,
538 Version 5 (GEOS-5) to forecast seasonal biosphere-atmosphere CO₂ fluxes in 2015-16 El Niño (Ott et al., 2018),
539 ~~and~~ used in NASA's Carbon Monitoring System as the tool for high spatial resolution (e.g., 90 m) regional forest
540 carbon modelling and monitoring (Hurt et al., 2019a; Ma et al., 2021), ~~and leveraged, and also~~ by NASA's Global
541 Ecosystem Dynamics Investigation mission for quantification of land carbon sequestration potential (Dubayah et al.,
542 2020a; Ma et al., 2020). Results from these studies will likely be of importance ~~to~~ for a range of science
543 applications, and ~~also be~~ used to inform and prioritize future model advances. Meanwhile, the increasing number of
544 remote sensing missions and related data sets, advances in computation, and growing stakeholder interests in carbon
545 and climate, as evidenced by the UN Paris Climate Agreement, bode well for future advances.

546
547 *Code and data availability.* All model simulation and source script can be found in
548 <https://doi.org/10.5281/zenodo.5236771>. All benchmarking datasets are cited and publicly available.

549
550 *Author contributions.* LM, GH, JF, SF and RS developed model code. LM, GH and LO designed this study. LM
551 conducted model simulation and evaluation. LM, GH and RL wrote main body of the manuscript. All authors
552 contributed to analysis and manuscript preparation.

553
554 *Competing interests.* The authors declare that they have no conflict of interest.

555
556 *Acknowledgements.* This work was funded by NASA-CMS (grant no. 80NSSC17K0710, 80NSSC20K0006, and
557 80NSSC21K1059), and NASA-IDS (grant no. 80NSSC17K0348).

558 **References**

559 Abramowitz, G.: Towards a public, standardized, diagnostic benchmarking system for land surface models, 5, 819–
560 827, <https://doi.org/10.5194/gmd-5-819-2012>, 2012.

561 Albani, M., Medvigy, D., Hurtt, G. C. and Moorcroft, P. R.: The contributions of land-use change, CO₂ fertilization,
562 and climate variability to the Eastern US carbon sink, *Global Change Biology*, 12(12), 2370–2390,
563 <https://doi.org/10.1111/j.1365-2486.2006.01254.x>, 2006.

564 Anav, A., Friedlingstein, P., Kidston, M., Bopp, L., Ciais, P., Cox, P., Jones, C., Jung, M., Myneni, R., and Zhu, Z.:
565 Evaluating the land and ocean components of the global carbon cycle in the CMIP5 earth system models, 26, 6801–
566 6843, 2013.

567 Ball, J. T., Woodrow, I. E., and Berry, J. A.: A model predicting stomatal conductance and its contribution to the
568 control of photosynthesis under different environmental conditions, in: *Progress in photosynthesis research*,
569 Springer, 221–224, 1987.

570 Beer, C., Reichstein, M., Tomelleri, E., Ciais, P., Jung, M., Carvalhais, N., Rödenbeck, C., Arain, M. A., Baldocchi,
571 D., Bonan, G. B., Bondeau, A., Cescatti, A., Lasslop, G., Lindroth, A., Lomas, M., Luyssaert, S., Margolis, H.,
572 Oleson, K. W., Rouspard, O., Veenendaal, E., Viovy, N., Williams, C., Woodward, F. I. and Papale, D.: Terrestrial
573 Gross Carbon Dioxide Uptake: Global Distribution and Covariation with Climate, *Science*, 329(5993), 834,
574 <https://doi.org/10.1126/science.1184984>, 2010.

575 Bernacchi, C. J., Singsaas, E. L., Pimentel, C., Jr, A. R. P. and Long, S. P.: Improved temperature response functions
576 for models of Rubisco-limited photosynthesis, *Plant, Cell & Environment*, 24(2), 253–259,
577 <https://doi.org/10.1111/j.1365-3040.2001.00668.x>, 2001.

578 Bonan, G. B.: Comparison of two land surface process models using prescribed forcings, 99, 25803–25818, 1994.

579 [Bonan, G. B., Patton, E. G., Finnigan, J. J., Baldocchi, D. D., and Harman, I. N.: Moving beyond the incorrect but](#)
580 [useful paradigm: reevaluating big-leaf and multilayer plant canopies to model biosphere-atmosphere fluxes – a](#)
581 [review, *Agricultural and Forest Meteorology*, 306, 108435, <https://doi.org/10.1016/j.agrformet.2021.108435>, 2021.](#)

582 Botkin, D. B., Janak, J. F. and Wallis, J. R.: Some ecological consequences of a computer model of forest growth,
583 *The Journal of Ecology*, 849–872, 1972.

584 Brovkin, V., Sitch, S., Von Bloh, W., Claussen, M., Bauer, E. and Cramer, W.: Role of land cover changes for
585 atmospheric CO₂ increase and climate change during the last 150 years, *Global Change Biology*, 10(8), 1253–1266,
586 <https://doi.org/10.1111/j.1365-2486.2004.00812.x>, 2004.

587 von Caemmerer, S. and Furbank, R. T.: Modeling C₄ photosynthesis, *C₄ plant biology*, 173–211, 1999.

588 von Caemmerer, S.: *Biochemical models of leaf photosynthesis*, Csiro publishing., 2000.

589 von Caemmerer, S., Farquhar, G. and Berry, J.: Biochemical Model of C₃ Photosynthesis, in *Photosynthesis in*
590 *silico: Understanding Complexity from Molecules to Ecosystems*, edited by A. Laisk, L. Nedbal, and Govindjee, pp.
591 209–230, Springer Netherlands, Dordrecht, https://doi.org/10.1007/978-1-4020-9237-4_9, , 2009.

592 Canadell, J. G., Kirschbaum, M. U. F., Kurz, W. A., Sanz, M.-J., Schlamadinger, B. and Yamagata, Y.: Factoring
593 out natural and indirect human effects on terrestrial carbon sources and sinks, *Environmental Science & Policy*,
594 10(4), 370–384, <https://doi.org/10.1016/j.envsci.2007.01.009>, 2007.

595 Chevallier, F., Fisher, M., Peylin, P., Serrar, S., Bousquet, P., Bréon, F.-M., Chédin, A. and Ciais, P.: Inferring CO₂
596 sources and sinks from satellite observations: Method and application to TOVS data, *Journal of Geophysical*
597 *Research: Atmospheres*, 110(D24), <https://doi.org/10.1029/2005JD006390>, 2005.

598 Chini, L., Hurtt, G., Sahajpal, R., Frohling, S., Klein Goldewijk, K., Sitch, S., Ganzenmüller, R., Ma, L., Ott, L. and
599 Pongratz, J.: Land-Use Harmonization Datasets for Annual Global Carbon Budgets, *Earth System Science Data*
600 *Discussions*, 1–27, 2021.

601 Ciais, P., Sabine, C., Bala, G., Bopp, L., Brovkin, V., Canadell, J., Chhabra, A., DeFries, R., Galloway, J. and
602 Heimann, M.: Carbon and other biogeochemical cycles, in *Climate change 2013: the physical science basis*.

- 603 Contribution of Working Group I to the Fifth Assessment Report of the Intergovernmental Panel on Climate
604 Change, pp. 465–570, Cambridge University Press, , 2014a.
- 605 Ciais, P., Dolman, A. J., Bombelli, A., Duren, R., Pregon, A., Rayner, P. J., Miller, C., Gobron, N., Kinderman, G.,
606 Marland, G., Gruber, N., Chevallier, F., Andres, R. J., Balsamo, G., Bopp, L., Bréon, F.-M., Broquet, G., Dargaville,
607 R., Battin, T. J., Borges, A., Bovensmann, H., Buchwitz, M., Butler, J., Canadell, J. G., Cook, R. B., DeFries, R.,
608 Engelen, R., Gurney, K. R., Heinze, C., Heimann, M., Held, A., Henry, M., Law, B., Luysaert, S., Miller, J.,
609 Moriyama, T., Moulin, C., Myneni, R. B., Nussli, C., Obersteiner, M., Ojima, D., Pan, Y., Paris, J.-D., Piao, S. L.,
610 Poulter, B., Plummer, S., Quegan, S., Raymond, P., Reichstein, M., Rivier, L., Sabine, C., Schimel, D., Tarasova,
611 O., Valentini, R., Wang, R., van der Werf, G., Wickland, D., Williams, M., and Zehner, C.: Current systematic
612 carbon-cycle observations and the need for implementing a policy-relevant carbon observing system, 11, 3547–
613 3602, <https://doi.org/10.5194/bg-11-3547-2014>, 2014b.
- 614 Collatz, G. J., Ball, J. T., Grivet, C., and Berry, J. A.: Physiological and environmental regulation of stomatal
615 conductance, photosynthesis and transpiration: a model that includes a laminar boundary layer, 54, 107–136, 1991.
- 616 Collatz, G. J., Ribas-Carbo, M., and Berry, J. A.: Coupled photosynthesis-stomatal conductance model for leaves of
617 C4 plants, 19, 519–538, 1992.
- 618 Collier, N., Hoffman, F. M., Lawrence, D. M., Keppel-Aleks, G., Koven, C. D., Riley, W. J., Mu, M., and
619 Randerson, J. T.: The International Land Model Benchmarking (ILAMB) System: Design, Theory, and
620 Implementation, 10, 2731–2754, <https://doi.org/10.1029/2018MS001354>, 2018.
- 621 Cramer, W., Bondeau, A., Woodward, F. I., Prentice, I. C., Betts, R. A., Brovkin, V., Cox, P. M., Fisher, V., Foley,
622 J. A., Friend, A. D., Kucharik, C., Lomas, M. R., Ramankutty, N., Sitch, S., Smith, B., White, A. and Young-
623 Molling, C.: Global response of terrestrial ecosystem structure and function to CO2 and climate change: results from
624 six dynamic global vegetation models, *Global Change Biology*, 7(4), 357–373, <https://doi.org/10.1046/j.1365-2486.2001.00383.x>, 2001.
- 626 Dickinson, R. E.: Biosphere atmosphere transfer scheme (BATS) version 1e as coupled to the NCAR community
627 climate model, 1993.
- 628 Dubayah, R., Blair, J. B., Goetz, S., Fatoyinbo, L., Hansen, M., Healey, S., Hofton, M., Hurtt, G., Kellner, J.,
629 Luthcke, S., Armston, J., Tang, H., Duncanson, L., Hancock, S., Jantz, P., Marselis, S., Patterson, P. L., Qi, W. and
630 Silva, C.: The Global Ecosystem Dynamics Investigation: High-resolution laser ranging of the Earth’s forests and
631 topography, *Science of Remote Sensing*, 1, 100002, <https://doi.org/10.1016/j.srs.2020.100002>, 2020a.
- 632 Dubayah, R., Tang, H., Armston, J., Luthcke, S., Hofton, M. and Blair, J.: GEDI L2B Canopy Cover and Vertical
633 Profile Metrics Data Global Footprint Level V001, , https://doi.org/10.5067/GEDI/GEDI02_B.001, 2020b.
- 634 Dubayah, R., Hofton, M., Blair, J., Armston, J., Tang, H. and Luthcke, S.: GEDI L2A Elevation and Height Metrics
635 Data Global Footprint Level V001, , https://doi.org/10.5067/GEDI/GEDI02_A.001, 2020c.
- 636 Erb, K.-H., Kastner, T., Luysaert, S., Houghton, R. A., Kuemmerle, T., Olofsson, P. and Haberl, H.: Bias in the
637 attribution of forest carbon sinks, *Nature Climate Change*, 3(10), 854–856, <https://doi.org/10.1038/nclimate2004>,
638 2013.
- 639 ESA: Land Cover CCI Product User Guide Version 2. Tech. Rep., Available at:
640 maps.elie.ucl.ac.be/CCI/viewer/download/ESACCI-LC-Ph2-PUGv2_2.0.pdf, 2017.
- 641 [Eyring, V., Cox, P. M., Flato, G. M., Gleckler, P. J., Abramowitz, G., Caldwell, P., Collins, W. D., Gier, B. K., Hall,](#)
642 [A. D., Hoffman, F. M., Hurtt, G. C., Jahn, A., Jones, C. D., Klein, S. A., Krasting, J. P., Kwiatkowski, L., Lorenz,](#)
643 [R., Maloney, E., Meehl, G. A., Pendergrass, A. G., Pincus, R., Ruane, A. C., Russell, J. L., Sanderson, B. M.,](#)
644 [Santer, B. D., Sherwood, S. C., Simpson, I. R., Stouffer, R. J., and Williamson, M. S.: Taking climate model](#)
645 [evaluation to the next level, *Nature Clim Change*, 9, 102–110, <https://doi.org/10.1038/s41558-018-0355-y>, 2019.](#)

- 646 [Eyring, V., Gleckler, P. J., Heinze, C., Stouffer, R. J., Taylor, K. E., Balaji, V., Guilyardi, E., Joussaume, S.,](#)
647 [Kindermann, S., Lawrence, B. N., Meehl, G. A., Righi, M., and Williams, D. N.: Towards improved and more](#)
648 [routine Earth system model evaluation in CMIP, 7, 813–830, <https://doi.org/10.5194/esd-7-813-2016>, 2016.](#)
- 649 Farjon, A. and Filer, D.: An Atlas of the World's Conifers: An Analysis of their Distribution, Biogeography,
650 Diversity and Conservation Status, Brill. <https://brill.com/view/title/20587>, last access: 22 December 2020, 2013.
- 651 Farquhar, G. D., von Caemmerer, S. and Berry, J. A.: A biochemical model of photosynthetic CO₂ assimilation in
652 leaves of C₃ species, *Planta*, 149(1), 78–90, <https://doi.org/10.1007/BF00386231>, 1980.
- 653 Farquhar, G. D. and Sharkey, T. D.: Stomatal conductance and photosynthesis, 33, 317–345, 1982.
- 654 Fisher, R. A., Muszala, S., Verstein, M., Lawrence, P., Xu, C., McDowell, N. G., Knox, R. G., Koven, C., Holm,
655 J. and Rogers, B. M.: Taking off the training wheels: the properties of a dynamic vegetation model without climate
656 envelopes, *CLM4. 5 (ED)*, *Geoscientific Model Development*, 8(11), 3593–3619, 2015.
- 657 Fisher, R. A., Koven, C. D., Anderegg, W. R. L., Christoffersen, B. O., Dietze, M. C., Farrior, C. E., Holm, J. A.,
658 Hurtt, G. C., Knox, R. G., Lawrence, P. J., Lichstein, J. W., Longo, M., Matheny, A. M., Medvigy, D., Muller-
659 Landau, H. C., Powell, T. L., Serbin, S. P., Sato, H., Shuman, J. K., Smith, B., Trugman, A. T., Viskari, T.,
660 Verbeeck, H., Weng, E., Xu, C., Xu, X., Zhang, T. and Moorcroft, P. R.: Vegetation demographics in Earth System
661 Models: A review of progress and priorities, *Global Change Biology*, 24(1), 35–54,
662 <https://doi.org/10.1111/gcb.13910>, 2018.
- 663 Fisk, J. P.: Net effects of disturbance: Spatial, temporal, and soci-etal dimensions of forest disturbance and recovery
664 on terrestrial car-bon balance, Ph.D thesis, University of Maryland, College Park, Maryland, 2015.
- 665 Fisk, J. P., Hurtt, G. C., Chambers, J. Q., Zeng, H., Dolan, K. A. and Negrón-Juárez, R. I.: The impacts of tropical
666 cyclones on the net carbon balance of eastern US forests (1851–2000), *Environ. Res. Lett.*, 8(4), 045017,
667 <https://doi.org/10.1088/1748-9326/8/4/045017>, 2013.
- 668 Flanagan, S. A., Hurtt, G. C., Fisk, J. P., Sahajpal, R., Zhao, M., Dubayah, R., Hansen, M. C., Sullivan, J. H. and
669 Collatz, G. J.: Potential Transient Response of Terrestrial Vegetation and Carbon in Northern North America from
670 Climate Change, *Climate*, 7(9), 113, <https://doi.org/10.3390/cli7090113>, 2019.
- 671 Foley, J. A., Prentice, I. C., Ramankutty, N., Levis, S., Pollard, D., Sitch, S., and Haxeltine, A.: An integrated
672 biosphere model of land surface processes, terrestrial carbon balance, and vegetation dynamics, 10, 603–628, 1996.
- 673 Friedlingstein, P., O'Sullivan, M., Jones, M. W., Andrew, R. M., Hauck, J., Olsen, A., Peters, G. P., Peters, W.,
674 Pongratz, J. and Sitch, S.: Global carbon budget 2020, *Earth System Science Data*, 12(4), 3269–3340, 2020.
- 675 Gelaro, R., McCarty, W., Suárez, M. J., Todling, R., Molod, A., Takacs, L., Randles, C. A., Darmenov, A.,
676 Bosilovich, M. G., Reichle, R., Wargan, K., Coy, L., Cullather, R., Draper, C., Akella, S., Buchard, V., Conaty, A.,
677 da Silva, A. M., Gu, W., Kim, G.-K., Koster, R., Lucchesi, R., Merkova, D., Nielsen, J. E., Partyka, G., Pawson, S.,
678 Putman, W., Rienecker, M., Schubert, S. D., Sienkiewicz, M. and Zhao, B.: The Modern-Era Retrospective Analysis
679 for Research and Applications, Version 2 (MERRA-2), *J. Climate*, 30(14), 5419–5454,
680 <https://doi.org/10.1175/JCLI-D-16-0758.1>, 2017.
- 681 [Ghimire, B., Riley, W. J., Koven, C. D., Mu, M., and Randerson, J. T.: Representing leaf and root physiological](#)
682 [traits in CLM improves global carbon and nitrogen cycling predictions, 8, 598–613,](#)
683 <https://doi.org/10.1002/2015MS000538>, 2016.
- 684 Guanter, L., Zhang, Y., Jung, M., Joiner, J., Voigt, M., Berry, J. A., Frankenberg, C., Huete, A. R., Zarco-Tejada, P.,
685 Lee, J.-E., Moran, M. S., Ponce-Campos, G., Beer, C., Camps-Valls, G., Buchmann, N., Gianelle, D., Klumpp, K.,
686 Cescatti, A., Baker, J. M. and Griffis, T. J.: Global and time-resolved monitoring of crop photosynthesis with
687 chlorophyll fluorescence, *PNAS*, 111(14), E1327–E1333, <https://doi.org/10.1073/pnas.1320008111>, 2014.
- 688 Hansis, E., Davis, S. J. and Pongratz, J.: Relevance of methodological choices for accounting of land use change
689 carbon fluxes, *Global Biogeochemical Cycles*, 29(8), 1230–1246, <https://doi.org/10.1002/2014GB004997>, 2015.

- 690 Haxeltine, A. and Prentice, I. C.: BIOME3: An equilibrium terrestrial biosphere model based on ecophysiological
691 constraints, resource availability, and competition among plant functional types, 10, 693–709, 1996.
- 692 Hurtt, G. C., Moorcroft, P. R., Pacala, S. W. and Levin, S. A.: Terrestrial models and global change: challenges for
693 the future, *Global Change Biology*, 4(5), 581–590, <https://doi.org/10.1046/j.1365-2486.1998.t01-1-00203.x>, 1998.
- 694 Hurtt, G. C., Pacala, S. W., Moorcroft, P. R., Caspersen, J., Shevliakova, E., Houghton, R. A. and Moore, B.:
695 Projecting the future of the U.S. carbon sink, *PNAS*, 99(3), 1389–1394, <https://doi.org/10.1073/pnas.012249999>,
696 2002.
- 697 Hurtt, G. C., Dubayah, R., Drake, J., Moorcroft, P. R., Pacala, S. W., Blair, J. B. and Fearon, M. G.: Beyond
698 Potential Vegetation: Combining Lidar Data and a Height-Structured Model for Carbon Studies, *Ecological
699 Applications*, 14(3), 873–883, <https://doi.org/10.1890/02-5317>, 2004.
- 700 Hurtt, G. C., Fisk, J., Thomas, R. Q., Dubayah, R., Moorcroft, P. R. and Shugart, H. H.: Linking models and data on
701 vegetation structure, *Journal of Geophysical Research: Biogeosciences*, 115(G2),
702 <https://doi.org/10.1029/2009JG000937>, 2010.
- 703 Hurtt, G. C., Chini, L. P., Frohling, S., Betts, R., Feddema, J., Fischer, G., Fisk, J., Hibbard, K., Houghton, R., and
704 Janetos, A.: Harmonization of land-use scenarios for the period 1500–2100: 600 years of global gridded annual
705 land-use transitions, wood harvest, and resulting secondary lands, *Climatic change*, 109, 117–161, 2011.
- 706 Hurtt, G. C., Thomas, R. Q., Fisk, J. P., Dubayah, R. O. and Sheldon, S. L.: The Impact of Fine-Scale Disturbances
707 on the Predictability of Vegetation Dynamics and Carbon Flux, *PLOS ONE*, 11(4), e0152883,
708 <https://doi.org/10.1371/journal.pone.0152883>, 2016.
- 709 Hurtt, G. C., Zhao, M., Sahajpal, R., Armstrong, A., Birdsey, R., Campbell, E., Dolan, K., Dubayah, R., Fisk, J. P.,
710 Flanagan, S., Huang, C., Huang, W., Johnson, K., Lamb, R., Ma, L., Marks, R., O’Leary, D., O’Neil-Dunne, J.,
711 Swatantran, A. and Tang, H.: Beyond MRV: high-resolution forest carbon modeling for climate mitigation planning
712 over Maryland, USA, *Environ. Res. Lett.*, 14(4), 045013, <https://doi.org/10.1088/1748-9326/ab0bbe>, 2019a.
- 713 Hurtt, G., Chini, L., Sahajpal, R., Frohling, S., Bodirsky, B. L., Calvin, K., Doelman, J., Fisk, J., Fujimori, S.,
714 Goldewijk, K. K., Hasegawa, T., Havlik, P., Heinemann, A., Humpenöder, F., Jungclaus, J., Kaplan, J., Krisztin, T.,
715 Lawrence, D., Lawrence, P., Mertz, O., Pongratz, J., Popp, A., Riahi, K., Shevliakova, E., Stehfest, E., Thornton, P.,
716 van Vuuren, D., and Zhang, X.: input4MIPs.CMIP6.CMIP.UofMD,
717 <https://doi.org/10.22033/ESGF/input4MIPs.10454>, 2019b.
- 718 Hurtt, G. C., Chini, L., Sahajpal, R., Frohling, S., Bodirsky, B. L., Calvin, K., Doelman, J. C., Fisk, J., Fujimori, S.
719 and Klein Goldewijk, K.: Harmonization of global land use change and management for the period 850–2100
720 (LUH2) for CMIP6, *Geoscientific Model Development*, 13(11), 5425–5464, 2020.
- 721 [Ito, A., Hajima, T., Lawrence, D. M., Brovkin, V., Delire, C., Guenet, B., Jones, C. D., Malyshev, S., Matera, S.,](#)
722 [McDermid, S. P., Peano, D., Pongratz, J., Robertson, E., Shevliakova, E., Vuichard, N., Wärlind, D., Wiltshire, A.,](#)
723 [and Ziehn, T.: Soil carbon sequestration simulated in CMIP6-LUMIP models: implications for climatic mitigation,](#)
724 [Environ. Res. Lett., 15, 124061, <https://doi.org/10.1088/1748-9326/abc912>, 2020.](#)
- 725 [Jeong, S. J. and Medvigy, D.: Macroscale prediction of autumn leaf coloration throughout the continental United](#)
726 [States, *Global Ecology and Biogeography*, 23\(11\), 1245–1254, <https://doi.org/10.1111/geb.12206>, 2014.](#)
- 727 Joiner, J., Yoshida, Y., Zhang, Y., Duveiller, G., Jung, M., Lyapustin, A., Wang, Y. and Tucker, C. J.: Estimation of
728 Terrestrial Global Gross Primary Production (GPP) with Satellite Data-Driven Models and Eddy Covariance Flux
729 Data, *Remote Sensing*, 10(9), 1346, <https://doi.org/10.3390/rs10091346>, 2018.
- 730 Jung, M., Schwalm, C., Migliavacca, M., Walther, S., Camps-Valls, G., Koirala, S., Anthoni, P., Besnard, S.,
731 Bodesheim, P., Carvalhais, N., Chevallier, F., Gans, F., Goll, D. S., Haverd, V., Köhler, P., Ichii, K., Jain, A. K.,
732 Liu, J., Lombardozzi, D., Nabel, J. E. M. S., Nelson, J. A., O’Sullivan, M., Pallandt, M., Papale, D., Peters, W.,
733 Pongratz, J., Rödenbeck, C., Sitch, S., Tramontana, G., Walker, A., Weber, U. and Reichstein, M.: Scaling carbon

- 734 fluxes from eddy covariance sites to globe: synthesis and evaluation of the FLUXCOM approach, *Biogeosciences*,
735 17(5), 1343–1365, <https://doi.org/10.5194/bg-17-1343-2020>, 2020.
- 736 Kattge, J. and Knorr, W.: Temperature acclimation in a biochemical model of photosynthesis: a reanalysis of data
737 from 36 species, *Plant, Cell & Environment*, 30(9), 1176–1190, <https://doi.org/10.1111/j.1365-3040.2007.01690.x>,
738 2007.
- 739 [Kattge, J., Ogle, K., Bönisch, G., Díaz, S., Lavorel, S., Madin, J., Nadrowski, K., Nöller, S., Sartor, K., and Wirth,
740 C.: A generic structure for plant trait databases, 2, 202–213, <https://doi.org/10.1111/j.2041-210X.2010.00067.x>,
741 2011.](https://doi.org/10.1111/j.2041-210X.2010.00067.x)
- 742 Kattge, J., Bönisch, G., Díaz, S., Lavorel, S., Prentice, I. C., Leadley, P., Tautenhahn, S., Werner, G. D., Aakala, T.,
743 and Abedi, M.: TRY plant trait database—enhanced coverage and open access, 26, 119–188, 2020.
- 744 Keeling, R. F.: Recording Earth’s Vital Signs, *Science*, 319(5871), 1771, <https://doi.org/10.1126/science.1156761>,
745 2008.
- 746 Keenan, T. F. and Williams, C. A.: The Terrestrial Carbon Sink, *Annu. Rev. Environ. Resour.*, 43(1), 219–243,
747 <https://doi.org/10.1146/annurev-environ-102017-030204>, 2018.
- 748 van der Laan-Luijckx, I. T., van der Velde, I. R., van der Veen, E., Tsuruta, A., Stanislawski, K., Babenhauerheide,
749 A., Zhang, H. F., Liu, Y., He, W., Chen, H., Masarie, K. A., Krol, M. C. and Peters, W.: The CarbonTracker Data
750 Assimilation Shell (CTDAS) v1.0: implementation and global carbon balance 2001–2015, *Geoscientific Model
751 Development*, 10(7), 2785–2800, <https://doi.org/10.5194/gmd-10-2785-2017>, 2017.
- 752 Lawrence, D. M., Fisher, R. A., Koven, C. D., Oleson, K. W., Swenson, S. C., Bonan, G., Collier, N., Ghimire, B.,
753 van Kampenhou, L., and Kennedy, D.: The Community Land Model version 5: Description of new features,
754 benchmarking, and impact of forcing uncertainty, *Journal of Advances in Modeling Earth Systems*, 11, 4245–4287,
755 2019.
- 756 Lee, J.-E., Frankenberg, C., van der Tol, C., Berry, J. A., Guanter, L., Boyce, C. K., Fisher, J. B., Morrow, E.,
757 Worden, J. R., Asefi, S., Badgley, G. and Saatchi, S.: Forest productivity and water stress in Amazonia: observations
758 from GOSAT chlorophyll fluorescence, *Proceedings of the Royal Society B: Biological Sciences*, 280(1761),
759 20130171, <https://doi.org/10.1098/rspb.2013.0171>, 2013.
- 760 Lieth, H.: Modeling the primary productivity of the world, in: *Primary productivity of the biosphere*, Springer, 237–
761 263, 1975.
- 762 Longo, M., Knox, R. G., Medvigy, D. M., Levine, N. M., Dietze, M. C., Kim, Y., Swann, A. L. S., Zhang, K.,
763 Rollinson, C. R., Bras, R. L., Wofsy, S. C. and Moorcroft, P. R.: The biophysics, ecology, and biogeochemistry of
764 functionally diverse, vertically and horizontally heterogeneous ecosystems: the Ecosystem Demography model,
765 version 2.2 – Part 1: Model description, *Geoscientific Model Development*, 12(10), 4309–4346,
766 <https://doi.org/10.5194/gmd-12-4309-2019>, 2019a.
- 767 [Longo, M., Knox, R. G., Levine, N. M., Swann, A. L. S., Medvigy, D. M., Dietze, M. C., Kim, Y., Zhang, K.,
768 Bonal, D., Durban, B., Camargo, P. B., Hayek, M. N., Saleska, S. R., da Silva, R., Bras, R. L., Wofsy, S. C. and
769 Moorcroft, P. R.: The biophysics, ecology, and biogeochemistry of functionally diverse, vertically and horizontally
770 heterogeneous ecosystems: the Ecosystem Demography model, version 2.2 – Part 2: Model evaluation for tropical
771 South America, *Geoscientific Model Development*, 12\(10\), 4347–4374, <https://doi.org/10.5194/gmd-12-4347-2019>,
772 2019b.](https://doi.org/10.5194/gmd-12-4347-2019)
- 773 Luo, Y. Q., Randerson, J. T., Friedlingstein, P., Hibbard, K., Hoffman, F., Huntzinger, D., Jones, C. D., Koven, C.,
774 Lawrence, D., and Li, D. J.: A framework for benchmarking land models, 2012.
- 775 Ma, L., Hurtt, G., Ott, L., Sahajpal, R., Fisk, J., Flanagan, S., Poulter, B., Liang, S., Sullivan, J. and Dubayah, R.:
776 Global Ecosystem Demography Model (ED-global v1.0): Development, Calibration and Evaluation for NASA’s
777 Global Ecosystem Dynamics Investigation (GEDI), *Earth and Space Science Open Archive*,
778 <https://doi.org/10.1002/essoar.10505486.1>, 2020.

779 Ma, L., Hurtt, G., Tang, H., Lamb, R. L., Campbell, E., Dubayah, R. O., Guy, M., Huang, W., Lister, A. and Lu, J.:
780 High-resolution forest carbon modeling for climate mitigation planning over the RGGI region, USA, *Environmental*
781 *Research Letters*, <https://doi.org/10.1088/1748-9326/abe4f4>, 2021.

782 Markus, T., Neumann, T., Martino, A., Abdalati, W., Brunt, K., Csatho, B., Farrell, S., Fricker, H., Gardner, A.,
783 Harding, D., Jasinski, M., Kwok, R., Magruder, L., Lubin, D., Luthcke, S., Morison, J., Nelson, R.,
784 Neuenschwander, A., Palm, S., Popescu, S., Shum, C., Schutz, B. E., Smith, B., Yang, Y. and Zwally, J.: The Ice,
785 Cloud, and land Elevation Satellite-2 (ICESat-2): Science requirements, concept, and implementation, *Remote*
786 *Sensing of Environment*, 190, 260–273, <https://doi.org/10.1016/j.rse.2016.12.029>, 2017.

787 Massad, R.-S., Tuzet, A. and Bethenod, O.: The effect of temperature on C4-type leaf photosynthesis parameters,
788 *Plant, Cell & Environment*, 30(9), 1191–1204, <https://doi.org/10.1111/j.1365-3040.2007.01691.x>, 2007.

789 Massoud, E. C., Xu, C., Fisher, R. A., Knox, R. G., Walker, A. P., Serbin, S. P., Christoffersen, B. O., Holm, J. A.,
790 Kueppers, L. M., and Ricciuto, D. M.: Identification of key parameters controlling demographically structured
791 vegetation dynamics in a land surface model: CLM4. 5 (FATES), *Geoscientific Model Development*, 12, 4133–
792 4164, 2019.

793 Medvigy, D.: The State of the Regional Carbon Cycle: Results from a Constrained Coupled Ecosystem-atmosphere
794 Model, Ph.D thesis, Harvard University, Cambridge, Massachusetts
795 <https://books.google.com/books?id=ZJJwYgEACAAJ>, 2006.

796 Medvigy, D., Wofsy, S. C., Munger, J. W., Hollinger, D. Y. and Moorcroft, P. R.: Mechanistic scaling of ecosystem
797 function and dynamics in space and time: Ecosystem Demography model version 2, *Journal of Geophysical*
798 *Research: Biogeosciences*, 114(G1), <https://doi.org/10.1029/2008JG000812>, 2009.

799 Mercado, L. M., Bellouin, N., Sitch, S., Boucher, O., Huntingford, C., Wild, M. and Cox, P. M.: Impact of changes
800 in diffuse radiation on the global land carbon sink, *Nature*, 458(7241), 1014–1017, 2009.

801 Monteith, J.: Evaporation and environment, *Symposia of the Society for Experimental Biology*, 19, 205–234, 1965.

802 Montzka, C., Herbst, M., Weihermüller, L., Verhoef, A. and Vereecken, H.: A global data set of soil hydraulic
803 properties and sub-grid variability of soil water retention and hydraulic conductivity curves, *Earth System*
804 *Data*, 9(2), 529–543, 2017.

805 Moorcroft, P. R., Hurtt, G. C. and Pacala, S. W.: A Method for Scaling Vegetation Dynamics: The Ecosystem
806 Demography Model (ed), *Ecological Monographs*, 71(4), 557–586, [https://doi.org/10.1890/0012-9615\(2001\)071\[0557:AMFSVD\]2.0.CO;2](https://doi.org/10.1890/0012-9615(2001)071[0557:AMFSVD]2.0.CO;2), 2001.

807
808 [Morton, D. C., Nagol, J., Carabajal, C. C., Rosette, J., Palace, M., Cook, B. D., Vermote, E. F., Harding, D. J., and](https://doi.org/10.1038/nature13006)
809 [North, P. R. J.: Amazon forests maintain consistent canopy structure and greenness during the dry season, 506, 221–](https://doi.org/10.1038/nature13006)
810 [224, <https://doi.org/10.1038/nature13006>, 2014.](https://doi.org/10.1038/nature13006)

811 Mu, Q., Zhao, M., and Running, S. W.: Improvements to a MODIS global terrestrial evapotranspiration algorithm,
812 *Remote Sensing of Environment*, 115, 1781–1800, 2011.

813
814 Murray-Tortarolo, G., Anav, A., Friedlingstein, P., Sitch, S., Piao, S., Zhu, Z., Poulter, B., Zaehle, S., Ahlström, A.,
815 Lomas, M., Levis, S., Viovy, N. and Zeng, N.: Evaluation of Land Surface Models in Reproducing Satellite-Derived
816 LAI over the High-Latitude Northern Hemisphere. Part I: Uncoupled DGVMs, *Remote Sensing*, 5(10), 4819–4838,
817 <https://doi.org/10.3390/rs5104819>, 2013.

818 Myneni, R., Knyazikhin, Y. and Park: MCD15A3H MODIS/Terra+Aqua Leaf Area Index/FPAR 4-day L4 Global
819 500m SIN Grid V006, , <https://doi.org/10.5067/MODIS/MCD15A3H.006>, 2015.

820 Neilson, R. P.: A model for predicting continental-scale vegetation distribution and water balance, 5, 362–385,
821 1995.

- 822 Neuenschwander, A. L., Popescu, S. C., Nelson, R. F., Harding, D., Pitts, K. L. and Robbins, J.: ATLAS/ICESat-2
823 L3A Land and Vegetation Height, version 3, , <https://doi.org/10.5067/ATLAS/ATL08.003>, 2020.
- 824 Ott, L., Hurtt, G. C., Randerson, J. T., Chatterjee, A., Chen, Y., Chini, L. P., Davis, S. J., Hubacek, K., Lee, E., MA,
825 L., Poulter, B., Rousseaux, C. S., Sun, L., Woodard, D. and Zeng, F.: Toward integrated seasonal predictions of land
826 and ocean carbon flux: lessons from the 2015-16 El Nino, AGU Fall Meeting Abstracts, 51
827 <http://adsabs.harvard.edu/abs/2018AGUFM.B51E1990O>, last access: 24 November 2020, 2018.
- 828 Pacala, S. W., Canham, C. D., Saponara, J., Silander Jr, J. A., Kobe, R. K. and Ribbens, E.: Forest models defined
829 by field measurements: estimation, error analysis and dynamics, *Ecological monographs*, 66(1), 1–43, 1996.
- 830 Parton, W. J.: The CENTURY model, in: *Evaluation of soil organic matter models*, Springer, 283–291, 1996.
- 831 Peters, W., Jacobson, A. R., Sweeney, C., Andrews, A. E., Conway, T. J., Masarie, K., Miller, J. B., Bruhwiler, L.
832 M. P., Pétron, G., Hirsch, A. I., Worthy, D. E. J., van der Werf, G. R., Randerson, J. T., Wennberg, P. O., Krol, M.
833 C. and Tans, P. P.: An atmospheric perspective on North American carbon dioxide exchange: CarbonTracker, *Proc
834 Natl Acad Sci USA*, 104(48), 18925, <https://doi.org/10.1073/pnas.0708986104>, 2007.
- 835 Peylin, P., Law, R., Gurney, K., Chevallier, F., Jacobson, A., Maki, T., Niwa, Y., Patra, P., Peters, W. and Rayner,
836 P.: Global atmospheric carbon budget: results from an ensemble of atmospheric CO₂ inversions, *Biogeosciences*,
837 10(10), 6699–6720, 2013.
- 838 Pielke Sr., R. A., Pitman, A., Niyogi, D., Mahmood, R., McAlpine, C., Hossain, F., Goldewijk, K. K., Nair, U.,
839 Betts, R., Fall, S., Reichstein, M., Kabat, P. and de Noblet, N.: Land use/land cover changes and climate: modeling
840 analysis and observational evidence, *WIREs Climate Change*, 2(6), 828–850, <https://doi.org/10.1002/wcc.144>, 2011.
- 841 Potter, C. S., Randerson, J. T., Field, C. B., Matson, P. A., Vitousek, P. M., Mooney, H. A., and Klooster, S. A.:
842 Terrestrial ecosystem production: A process model based on global satellite and surface data, 7, 811–841,
843 <https://doi.org/10.1029/93GB02725>, 1993.
- 844 Poulter, B., MacBean, N., Hartley, A., Khlystova, I., Arino, O., Betts, R., Bontemps, S., Boettcher, M., Brockmann,
845 C., Defourny, P., Hagemann, S., Herold, M., Kirches, G., Lamarche, C., Lederer, D., Otlé, C., Peters, M. and
846 Peylin, P.: Plant functional type classification for earth system models: results from the European Space Agency’s
847 Land Cover Climate Change Initiative, *Geoscientific Model Development*, 8(7), 2315–2328,
848 <https://doi.org/10.5194/gmd-8-2315-2015>, 2015.
- 849 Prentice, I. C., Cramer, W., Harrison, S. P., Leemans, R., Monserud, R. A., and Solomon, A. M.: Special paper: a
850 global biome model based on plant physiology and dominance, soil properties and climate, 117–134, 1992.
- 851 Prentice, I. C. and Cowling, S. A.: Dynamic global vegetation models, *Encyclopedia of biodiversity*, 670–689,
852 <https://doi.org/10.1016/B978-0-12-384719-5.00412-3>, 2013.
- 853 Prentice, I. C., Bondeau, A., Cramer, W., Harrison, S. P., Hickler, T., Lucht, W., Sitch, S., Smith, B. and Sykes, M.
854 T.: Dynamic Global Vegetation Modeling: Quantifying Terrestrial Ecosystem Responses to Large-Scale
855 Environmental Change, in *Terrestrial Ecosystems in a Changing World*, edited by J. G. Canadell, D. E. Pataki, and
856 L. F. Pitelka, pp. 175–192, Springer, Berlin, Heidelberg, https://doi.org/10.1007/978-3-540-32730-1_15, , 2007.
- 857 Raich, J. W., Rastetter, E. B., Melillo, J. M., Kicklighter, D. W., Steudler, P. A., Peterson, B. J., Grace, A. L.,
858 Moore, B., and Vorosmarty, C. J.: Potential Net Primary Productivity in South America: Application of a Global
859 Model, 1, 399–429, <https://doi.org/10.2307/1941899>, 1991.
- 860 Randerson, J. T., Hoffman, F. M., Thornton, P. E., Mahowald, N. M., Lindsay, K., LEE, Y.-H., Nevison, C. D.,
861 Doney, S. C., Bonan, G., and Stöckli, R.: Systematic assessment of terrestrial biogeochemistry in coupled climate–
862 carbon models, 15, 2462–2484, 2009.
- 863 Randerson, J., Van Der Werf, G., Giglio, L., Collatz, G. and Kasibhatla, P.: Global Fire Emissions Database,
864 Version 4.1 (GFEDv4), ORNL DAAC, 2015.

- 865 Reich, P. B., Walters, M. B. and Ellsworth, D. S.: From tropics to tundra: Global convergence in plant functioning,
866 Proc Natl Acad Sci USA, 94(25), 13730, <https://doi.org/10.1073/pnas.94.25.13730>, 1997.
- 867 [Restrepo-Coupe, N., Levine, N. M., Christoffersen, B. O., Albert, L. P., Wu, J., Costa, M. H., Galbraith, D.,](#)
868 [Imbuzeiro, H., Martins, G., da Araujo, A. C., Malhi, Y. S., Zeng, X., Moorcroft, P., and Saleska, S. R.: Do dynamic](#)
869 [global vegetation models capture the seasonality of carbon fluxes in the Amazon basin? A data-model](#)
870 [intercomparison, 23, 191–208, <https://doi.org/10.1111/gcb.13442>, 2017.](#)
- 871 Rödenbeck, C., Le Quéré, C., Heimann, M. and Keeling, R. F.: Interannual variability in oceanic biogeochemical
872 processes inferred by inversion of atmospheric O₂/N₂ and CO₂ data, null, 60(5), 685–705,
873 <https://doi.org/10.1111/j.1600-0889.2008.00375.x>, 2008.
- 874 [Saleska, S. R., Wu, J., Guan, K., Araujo, A. C., Huete, A., Nobre, A. D., and Restrepo-Coupe, N.: Dry-season](#)
875 [greening of Amazon forests, 531, E4–E5, <https://doi.org/10.1038/nature16457>, 2016.](#)
- 876 Santoro, M., Cartus, O., Mermoz, S., Bouvet, A., Le Toan, T., Carvalhais, N., Rozendaal, D., Herold, M., Avitabile,
877 V., Quegan, S., Carreiras, J., Rauste, Y., Balzter, H., Schmillius, C. and Seifert, F. M.: GlobBiomass - global
878 datasets of forest biomass, , 174 data points, <https://doi.org/10.1594/PANGAEA.894711>, 2018.
- 879 Sato, H., Itoh, A., and Kohyama, T.: SEIB–DGVM: A new Dynamic Global Vegetation Model using a spatially
880 explicit individual-based approach, 200, 279–307, 2007.
- 881 Sellers, P. J., Mintz, Y., Sud, Y. C., and Dalcher, A.: A Simple Biosphere Model (SIB) for Use within General
882 Circulation Models, 43, 505–531, [https://doi.org/10.1175/1520-0469\(1986\)043<0505:ASBMFU>2.0.CO;2](https://doi.org/10.1175/1520-0469(1986)043<0505:ASBMFU>2.0.CO;2), 1986.
883
- 884 Shugart, H. H. and West, D.: Development of an Appalachian deciduous forest succession model and its application
885 to assessment of the impact of the chestnut blight., 1977.
- 886 Shugart, H. H., Wang, B., Fischer, R., Ma, J., Fang, J., Yan, X., Huth, A. and Armstrong, A. H.: Gap models and
887 their individual-based relatives in the assessment of the consequences of global change, Environmental Research
888 Letters, 13(3), 033001, <https://doi.org/10.1088/1748-9326/aaaacc>, 2018.
- 889 Sitch, S., Huntingford, C., Gedney, N., Levy, P. E., Lomas, M., Piao, S. L., Betts, R., Ciais, P., Cox, P.,
890 Friedlingstein, P., Jones, C. D., Prentice, I. C. and Woodward, F. I.: Evaluation of the terrestrial carbon cycle, future
891 plant geography and climate-carbon cycle feedbacks using five Dynamic Global Vegetation Models (DGVMs),
892 Global Change Biology, 14(9), 2015–2039, <https://doi.org/10.1111/j.1365-2486.2008.01626.x>, 2008.
- 893 Smith, B., Prentice, I. C., and Sykes, M. T.: Representation of vegetation dynamics in the modelling of terrestrial
894 ecosystems: comparing two contrasting approaches within European climate space, 621–637, 2001.
895
- 896 Smith, B., Wårlind, D., Arneth, A., Hickler, T., Leadley, P., Siltberg, J., and Zaehle, S.: Implications of
897 incorporating N cycling and N limitations on primary production in an individual-based dynamic vegetation model,
898 11, 2027–2054, 2014.
- 899 [Spafford, L. and MacDougall, A. H.: Validation of terrestrial biogeochemistry in CMIP6 Earth system models: a](#)
900 [review, Geosci. Model Dev., 14, 5863–5889, <https://doi.org/10.5194/gmd-14-5863-2021>, 2021.](#)
- 901 Spawn, S. A., Sullivan, C. C., Lark, T. J. and Gibbs, H. K.: Harmonized global maps of above and belowground
902 biomass carbon density in the year 2010, Scientific Data, 7(1), 112, <https://doi.org/10.1038/s41597-020-0444-4>,
903 2020.
- 904 [Tang, H. and Dubayah, R.: Light-driven growth in Amazon evergreen forests explained by seasonal variations of](#)
905 [vertical canopy structure, PNAS, 114, 2640–2644, <https://doi.org/10.1073/pnas.1616943114>, 2017.](#)
- 906 Todd-Brown, K. E. O., Randerson, J. T., Post, W. M., Hoffman, F. M., Tarnocai, C., Schuur, E. a. G. and Allison, S.
907 D.: Causes of variation in soil carbon simulations from CMIP5 Earth system models and comparison with
908 observations, Biogeosciences, 10(3), 1717–1736, <https://doi.org/10.5194/bg-10-1717-2013>, 2013.

- 909 Verger, A., Baret, F. and Weiss, M.: Near Real-Time Vegetation Monitoring at Global Scale, *IEEE Journal of*
910 *Selected Topics in Applied Earth Observations and Remote Sensing*, 7(8), 3473–3481,
911 <https://doi.org/10.1109/JSTARS.2014.2328632>, 2014.
- 912 Walther, G.-R., Post, E., Convey, P., Menzel, A., Parmesan, C., Beebee, T. J. C., Fromentin, J.-M., Hoegh-
913 Guldberg, O. and Bairlein, F.: Ecological responses to recent climate change, *Nature*, 416(6879), 389–395,
914 <https://doi.org/10.1038/416389a>, 2002.
- 915 Weng, E. S., Malyshev, S., Lichstein, J. W., Fariior, C. E., Dybzinski, R., Zhang, T., Shevliakova, E., and Pacala, S.
916 W.: Scaling from individual trees to forests in an Earth system modeling framework using a mathematically
917 tractable model of height-structured competition, 12, 2655–2694, 2015.
- 918 Wieder, W. R., Boehnert, J., Bonan, G. B. and Langseth, M.: RegridDED Harmonized World Soil Database v1.2,
919 ORNL DAAC, <https://doi.org/10.3334/ORNLDAAC/1247>, 2014.
- 920 Yang, X., Tang, J., Mustard, J. F., Lee, J.-E., Rossini, M., Joiner, J., Munger, J. W., Kornfeld, A. and Richardson, A.
921 D.: Solar-induced chlorophyll fluorescence that correlates with canopy photosynthesis on diurnal and seasonal
922 scales in a temperate deciduous forest, *Geophysical Research Letters*, 42(8), 2977–2987,
923 <https://doi.org/10.1002/2015GL063201>, 2015.
- 924 Zhang, Y., Joiner, J., Alemohammad, S. H., Zhou, S. and Gentine, P.: A global spatially contiguous solar-induced
925 fluorescence (CSIF) dataset using neural networks, *Biogeosciences*, 15(19), 5779–5800, 2018.
- 926
927

928 **Figures and Tables**

929

930 Table 1. Summary of benchmarking datasets used for evaluation of ED model.

931

Variable	Source	Description	Reference
Vegetation distribution			
PFT	ESA CCI	Global gridded, 300-m, 2015	ESA (2017)
Carbon stocks			
AGB	Santoro et al. (2018)	Global gridded, 100-m, 2010	Santoro et al. (2018)
	Spawn et al. (2020)	Global gridded, 300-m, 2010	Spawn et al. (2020)
Soil carbon	HWSD	Gridded, 0.05 degree, 2000	Wieder et al. (2014)
Carbon and water fluxes			
GPP	FLUXCOM (RS+METEO, CRUIA and ERA5)	Global gridded, 0.0833-degree, 1979-2017 monthly	Jung et al. (2020)
	FluxSat	Global gridded, 0.05-degree, 2001-2018 monthly	Joiner et al. (2018)
NBP	CAMS (v17r1)	Global gridded, 1.875x3.75-degree, 1979-2017 monthly	Chevallier et al. (2005)
	Jena CarbonScope (s81oc v2020)	Global gridded, 2.5x2.0 degree, 1981-2016 daily	Rödenbeck et al. (2008)
	CarbonTracker Europe (CTE)	Global gridded, 1x1 degree, 2000-2016 monthly	van der Laan-Luijkx et al. (2017)
	GCB2020 DGVMs	Global total, 1959-2019 yearly	Friedlingstein et al. (2020)
	GCB2020 Residual sink	Global total, 1959-2019 yearly	Friedlingstein et al. (2020)
ET	FLUXCOM (RS+METEO, CRUNCEP and GSWP3)	Global gridded, 0.0833-degree, 1981-2014 monthly	Jung et al. (2020)
Vegetation structure			
Tree height	GEDI L2A (v001 v002)	51°N ~ 51°S, 20-m footprint, 2019-2020	Dubayah et al. (2020c)
	ICESat-2 ATL08 (v003 v005)	51°N ~ 51°S, 100-m footprint, 2018-2020	Neuenschwander et al. (2020)
LAI	MODIS MCD15A3H (v006)	Global gridded, 500-m, 2003-2016 4-day	Myneni et al. (2015)
	GEOV2	Global gridded, 1/3-km, 1999-2016 10-day	Verger et al. (2014)
Vertical LAI	GEDI L2B (v001 v002)	51°N ~ 51°S, 20-m footprint, 2019-2020	Dubayah et al. (2020b)

932

933

934

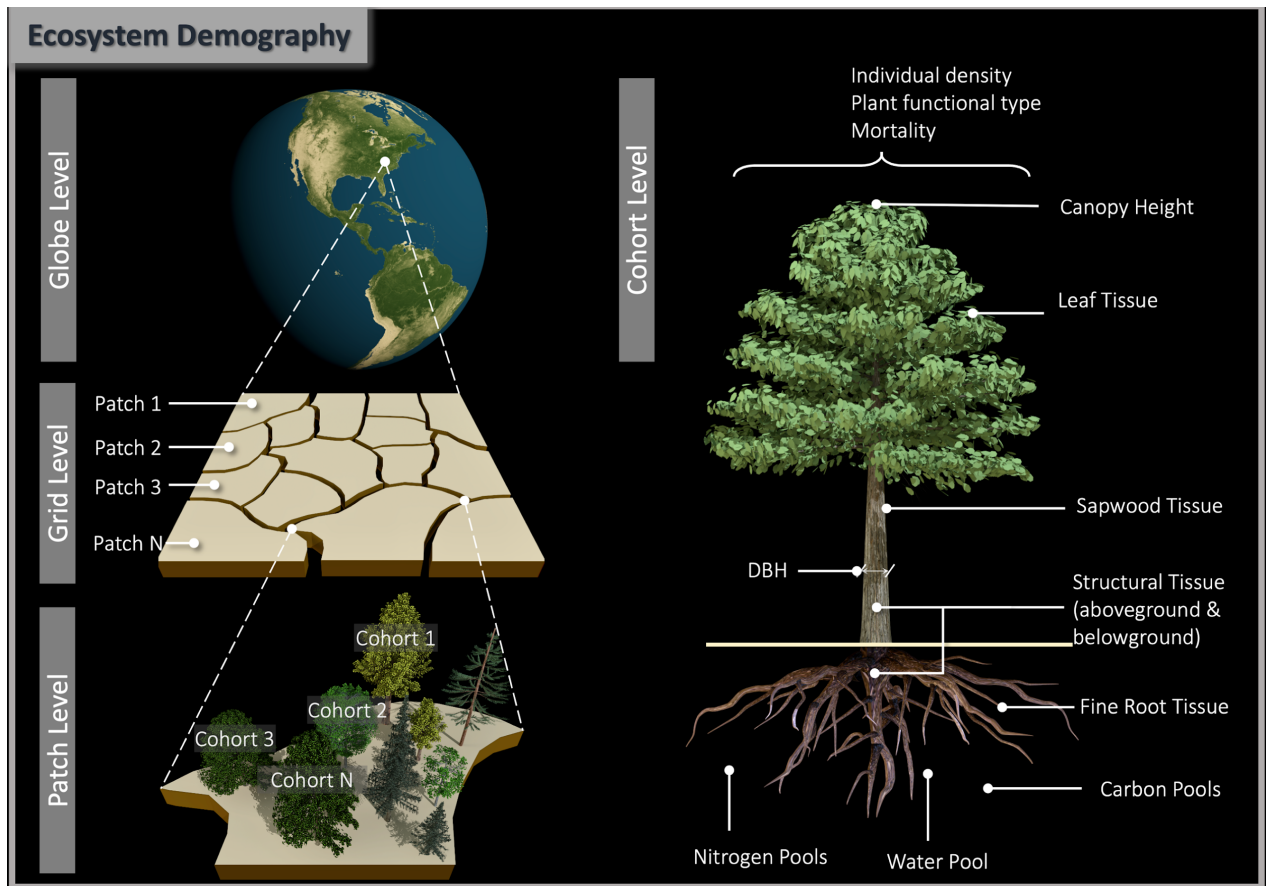


Figure 1. Diagram of vegetation representation scheme in ED model. Globe consists of land grids with fixed spatial resolution. A grid consists of patches with different ages from last disturbance and land use types, and patch areas dynamically change over time as a result of disturbance and land use changes. A patch consists of consists with different plant functional types and sizes. Plants in a cohort are depicted by properties including individual density, canopy height, diameter at breast (DBH), and biomass in leaf, sapwood, structural tissue and fine roots, and all these properties are simulated as a result of interaction with environment and other cohorts. Note that not all properties are shown here.

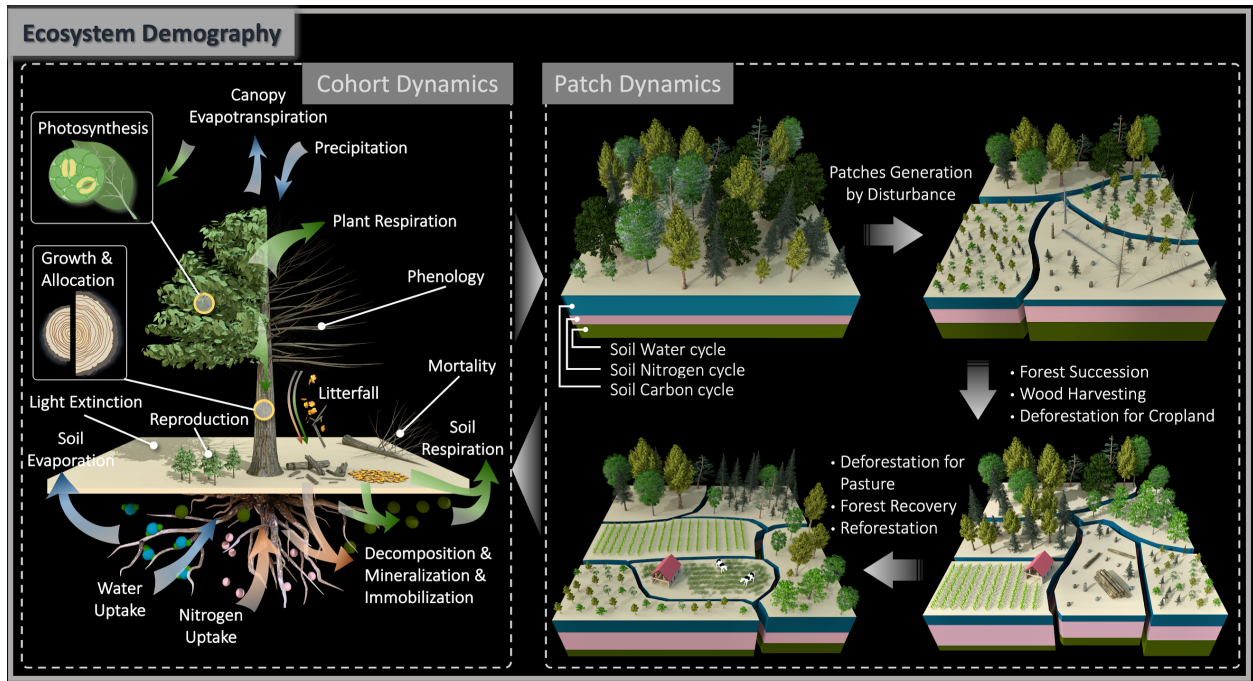


Figure 2. Schematic diagram of processes represented in ED model. Dynamics at cohort level consists of carbon-related flow (green arrow), water-related flow (blue arrow) and nitrogen-related (orange arrow). Carbon dynamics include carbon assimilation by photosynthesis, carbon allocation for plant growth in height/DBH, reproduction and respiration, carbon translocation between plants and soil through tissue turnover as litterfall and dead plants due to mortality, and carbon decomposition and respiration in soil carbon pools. Water dynamics include water inputs from precipitation and infiltration into soil, uptake by vegetation and evaporation and transpiration of soil and canopy. Nitrogen dynamics includes nitrogen uptake from soil pools, translocation from vegetation to soil through litterfall and dead plants, and mineralization and immobilization in soil. Note that not all processes that ED characterize are depicted here. Dynamics at patch level consist of consequences from a variety of disturbance events both natural and anthropogenic. Patch dynamics include disturbance-driven patch heterogenization in age and areas, forest succession, wood harvesting, deforestation for cropland and pasture expansion, and forest recovery and reforestation from abandoned cropland, harvested forest and pasture.

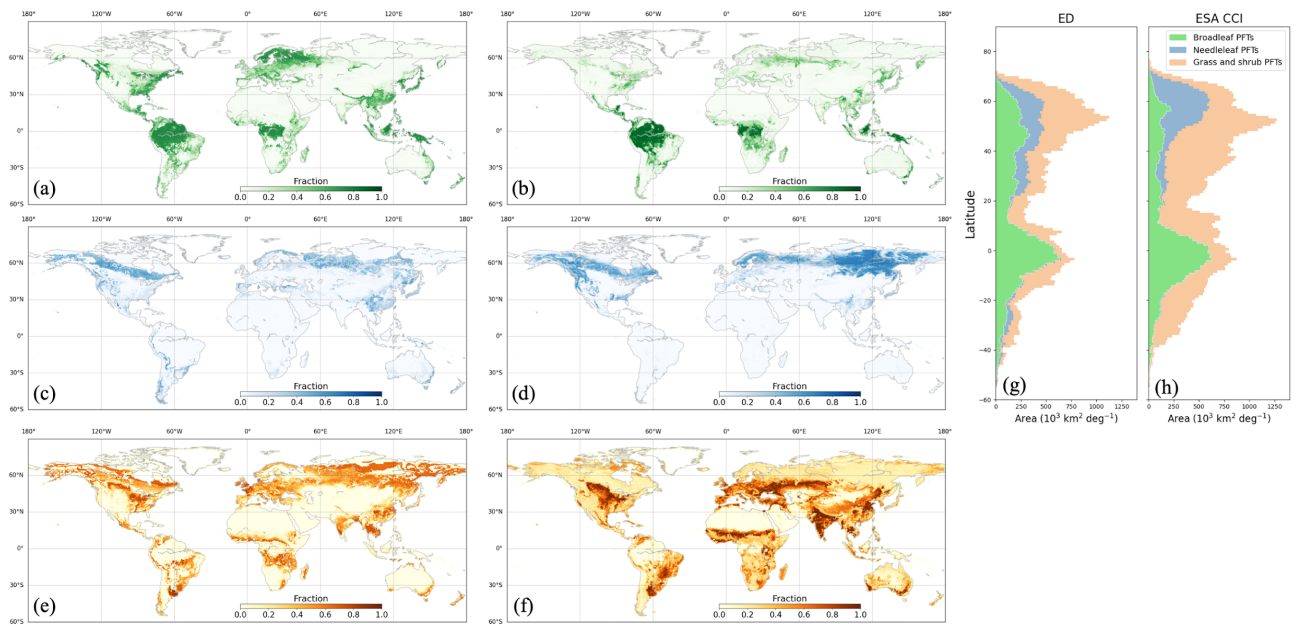


Figure 3. Spatial distribution of broadleaf PFTs, needleleaf and PFTs and grass and shrub PFTs in 2015 from ED (a), (c) and (e), and from ESA CCI (b), (d) and (f). Corresponding latitudinal total area is compared in (g) and (h).

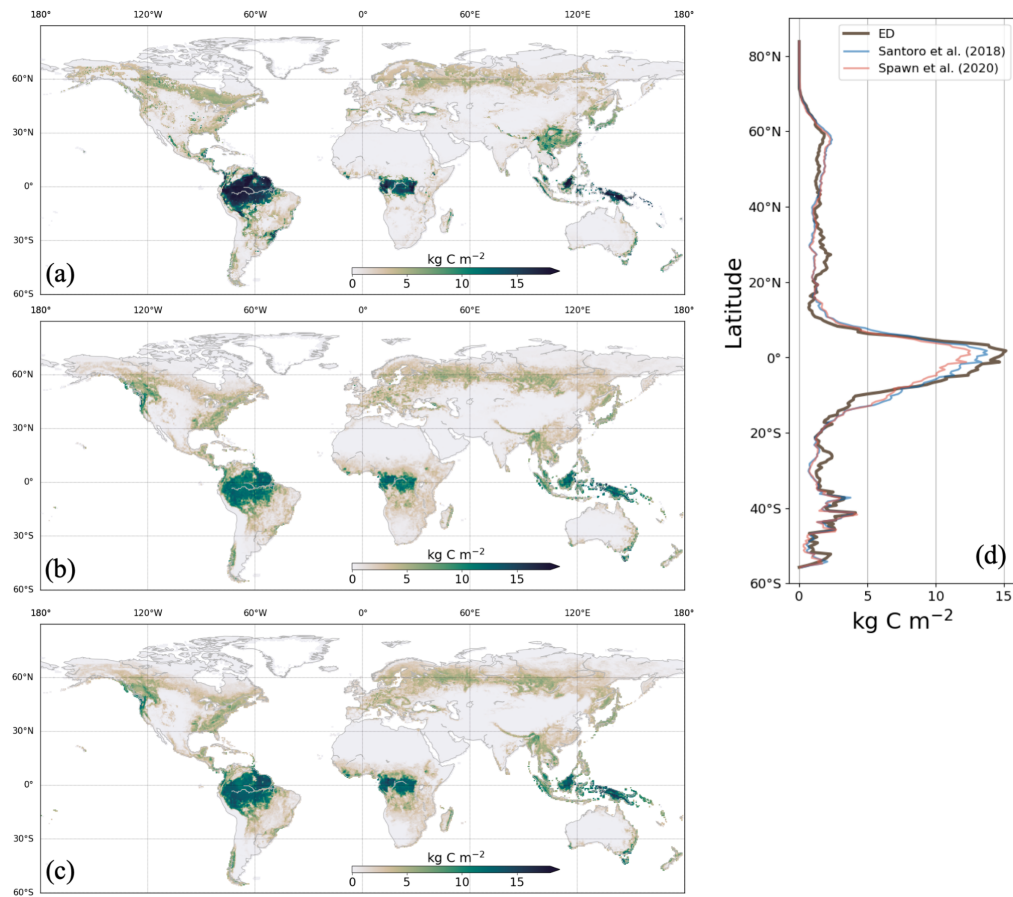


Figure 4. AGB in 2010 from ED (a), Spawn et al., (2020) (b), and Santoro et al., (2018) (c), with latitudinal average AGB compared in (d).

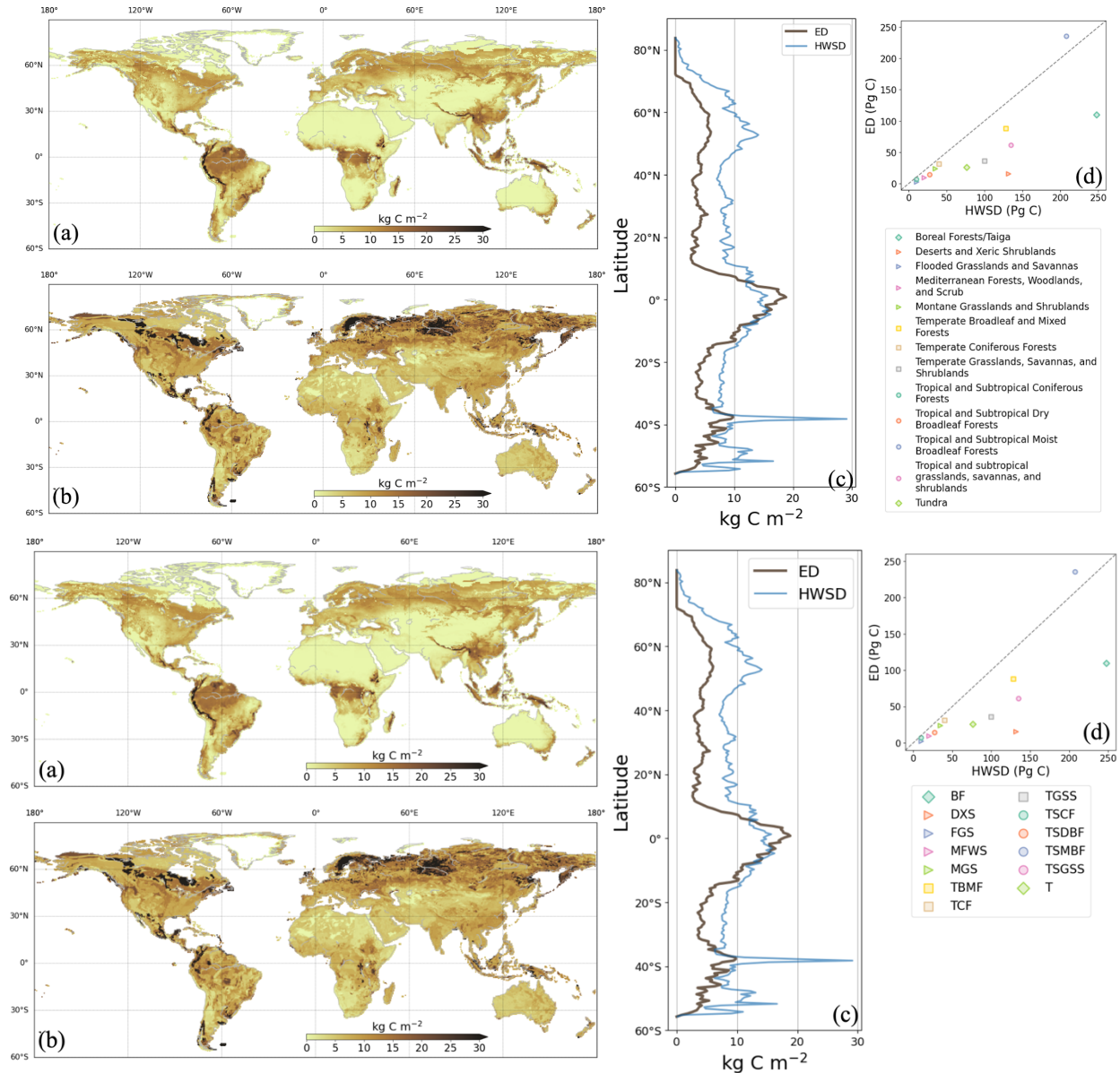


Figure 5. Soil carbon density in 2000 from ED (a) and HWSD (b). Latitudinal average density and total stocks per biome are compared in (c) and (d), respectively. In the legend of (d), BF is Boreal Forests/Taiga, DXS is Deserts and Xeric Shrublands, FGS is Flooded Grasslands and Savannas, MFWS is Mediterranean Forests, Woodlands, and Scrub, MGS is Montane Grasslands and Shrublands, TBMF is Temperate Broadleaf and Mixed Forests, TCF is Temperate Coniferous Forests, TGSS is Temperate Grasslands, Savannas, and Shrublands, TSCF is Tropical and Subtropical Coniferous Forests, TSDBF is Tropical and Subtropical Dry Broadleaf Forests, TSMBF is Tropical and Subtropical Moist Broadleaf Forests, TSGSS is Tropical and subtropical grasslands, savannas, and shrublands, and T is Tundra.

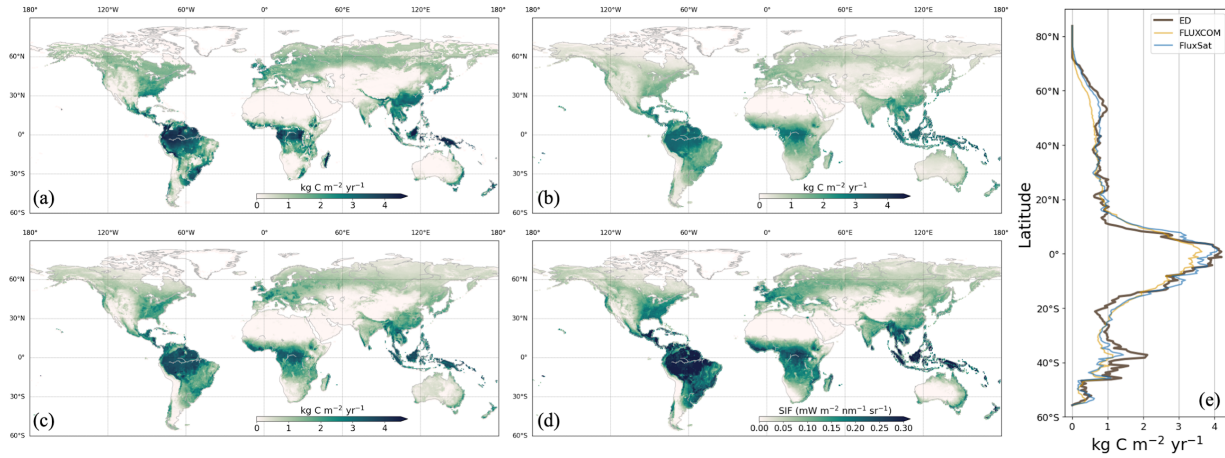


Figure 6. Average annual GPP between 2001 and 2016 from ED (a), FLUXCOM (b), FluxSat (c) and CSIF (d). Comparison of latitudinal average GPP is shown in (e).

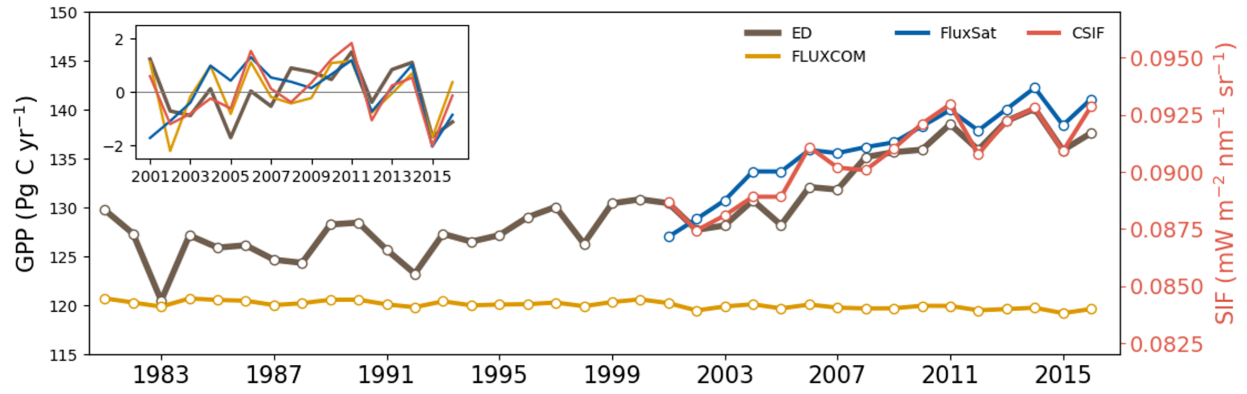


Figure 7. Time-series of global annual total GPP from ED, FLUXCOM, and FluxSat, and global annual average CSIF. Their interannual anomaly is shown in the inset.

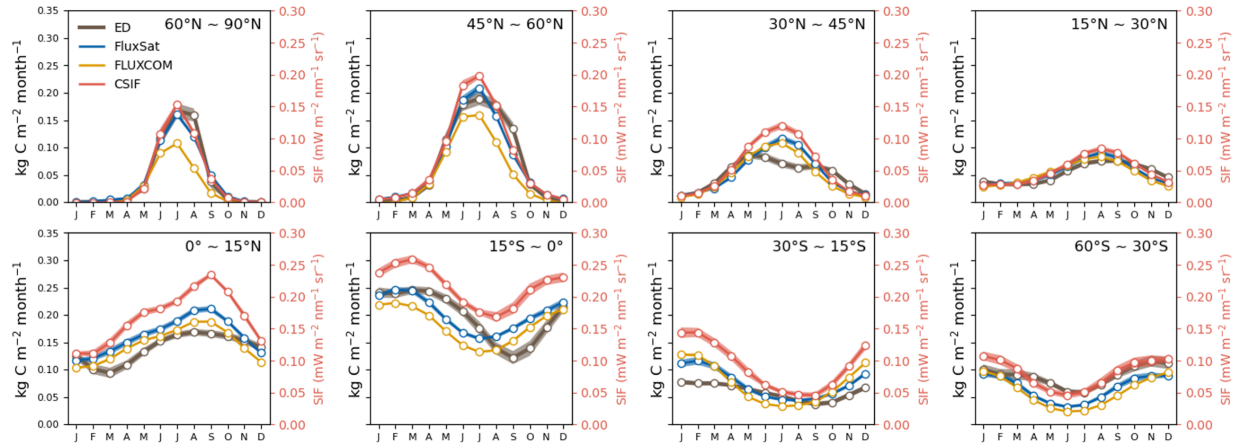


Figure 8. Average seasonal cycle (2001-2016) of GPP from ED, FLUXCOM, FluxSat, and CSIF by latitudinal band.

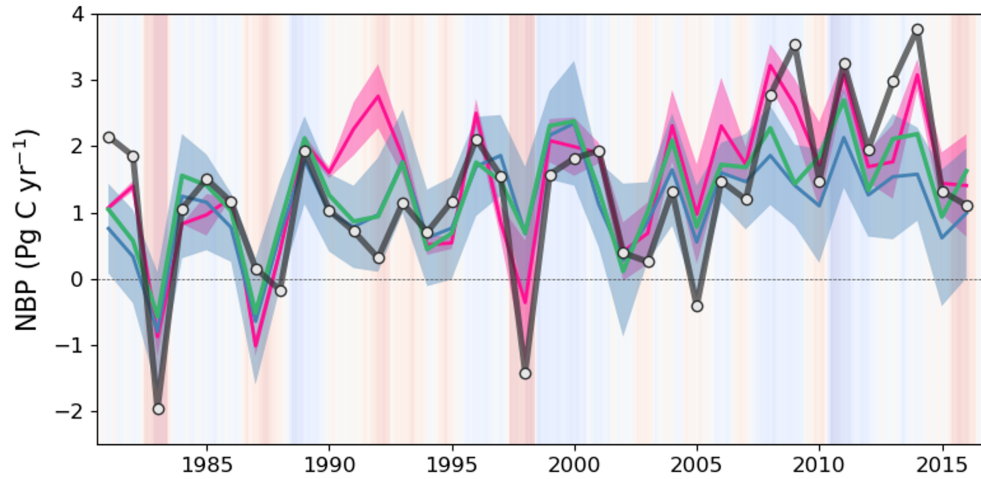


Figure 9. Global annual NBP between 1981 and 2016 from ED (black line), DGVMs from the GCB2020 (ensemble average shown in blue line with $\pm 1\sigma$ spread shown in blue shading), the ensemble of atmospheric inversions (ensemble average shown in pink line with $\pm 1\sigma$ spread shown in pink shading), and the terrestrial residual sink of the GCB2020 (green line). Positive values indicate net carbon uptake from land. Background shading represents the bi-monthly Multivariate El Niño/Southern Oscillation (ENSO) index, where red indicates El Niño and blue indicates La Niña.

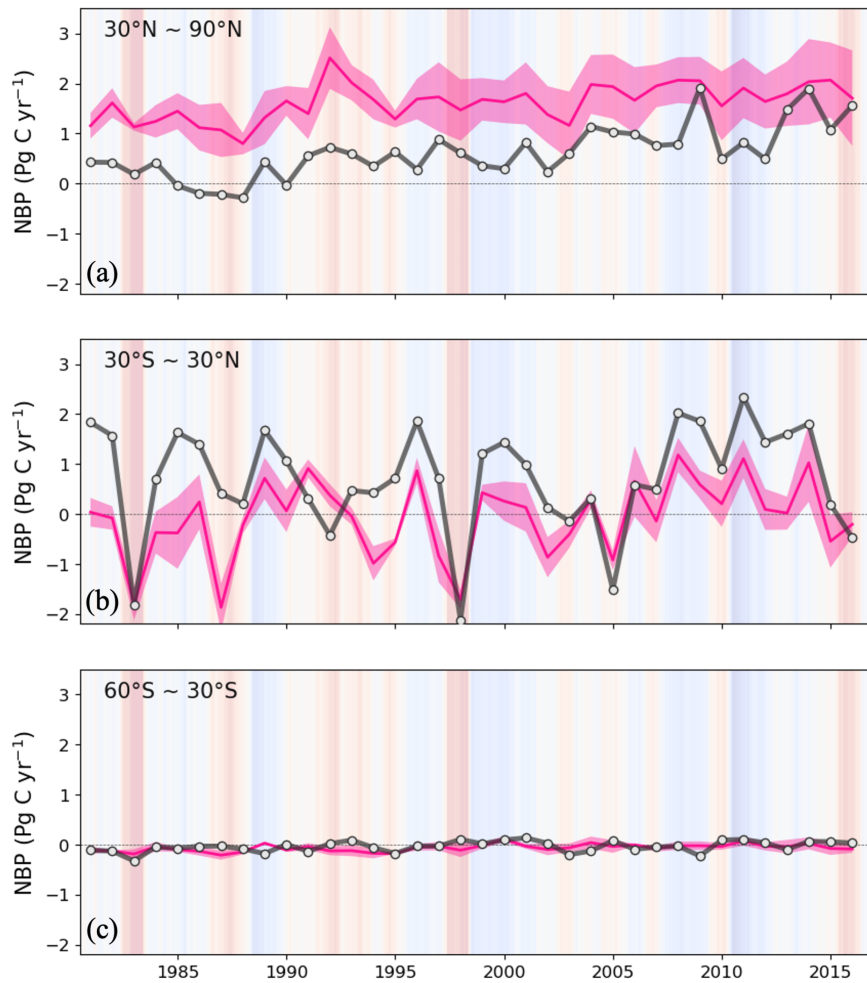


Figure 10. Annual NBP between 1981 and 2016 from ED and ensemble of atmospheric inversions for the Northern Hemisphere ($>30^\circ\text{N}$) (a), tropics ($30^\circ\text{N} - 30^\circ\text{S}$) (b) and the Southern Hemisphere ($<30^\circ\text{S}$) (c). Black line is ED, and the pink line and pink shading are the inversion ensemble average and $\pm 1\sigma$ spread of atmospheric inversions, respectively.

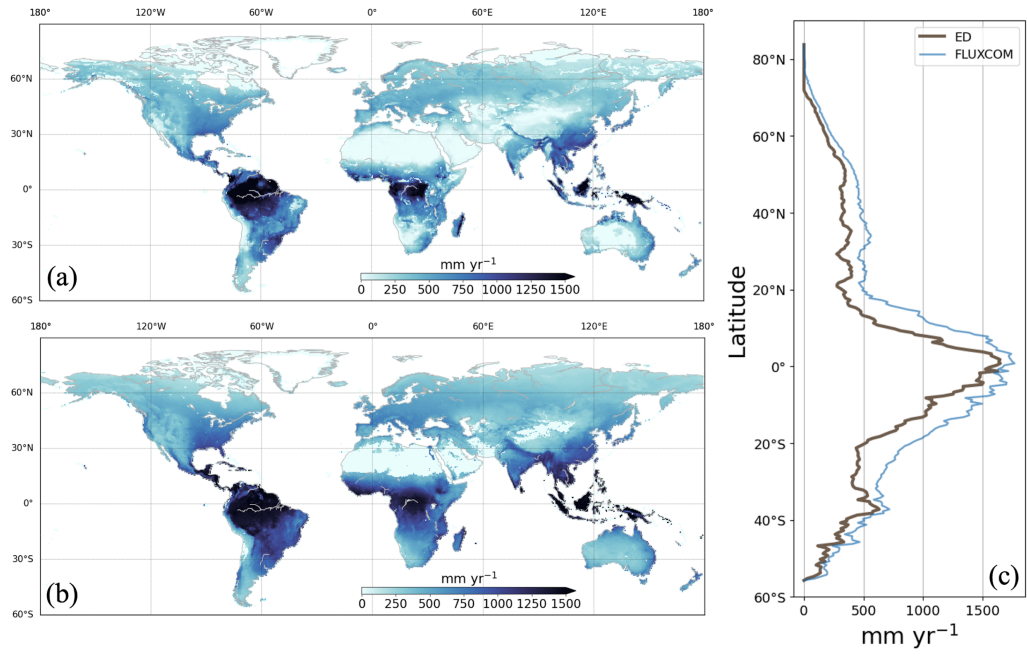


Figure 11. Average annual ET between 1981 and 2016 from ED (a) and FLUXCOM (b) with corresponding latitudinal average comparison (c).

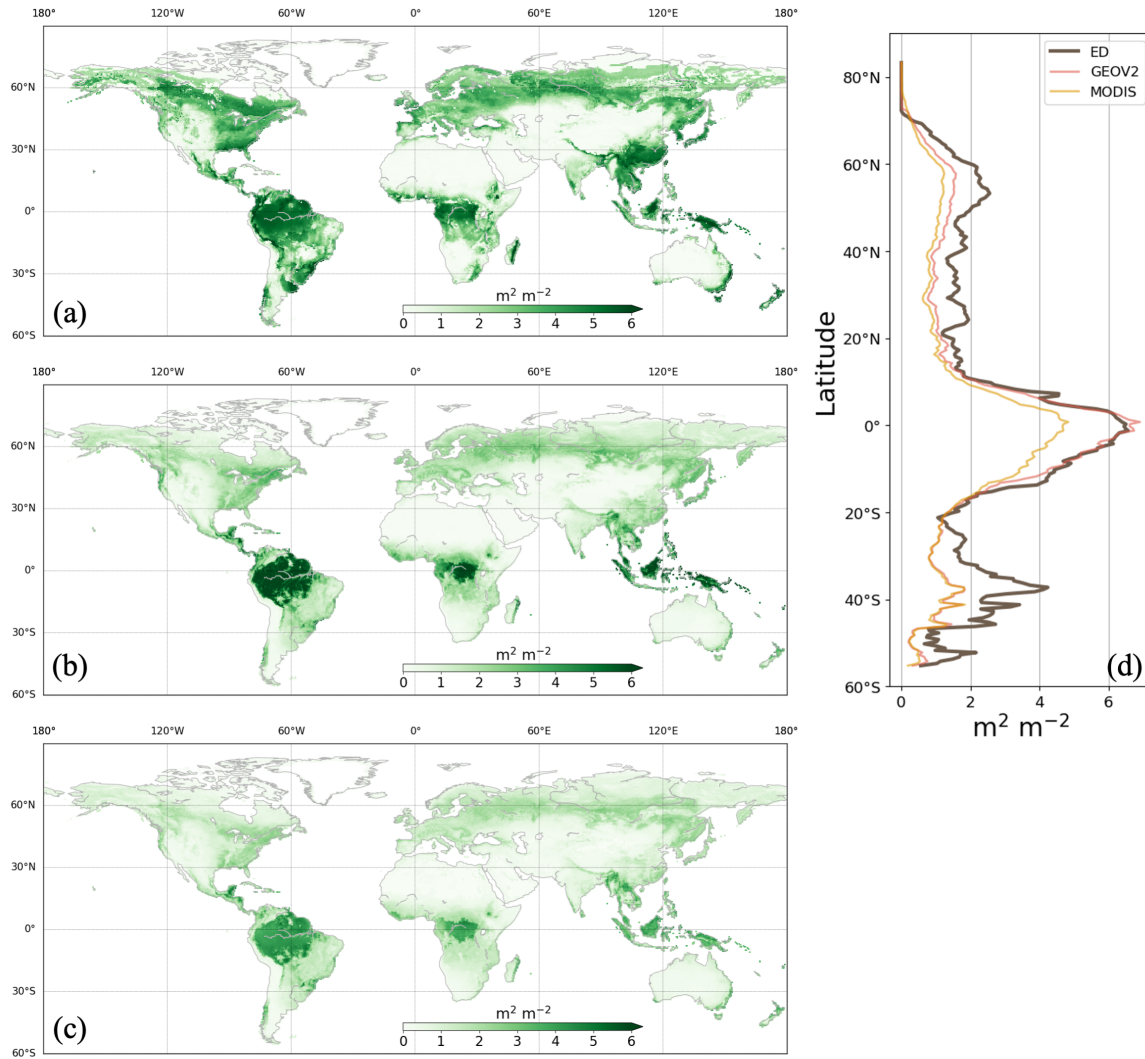


Figure 12. Average LAI during the growing season between 2003 and 2016 from ED (a), GEOV2 (b), and MODIS (c). Corresponding latitudinal averages are compared in (e). Growing season is defined as the months during which the average air temperature of MERRA2 is above 0°C.

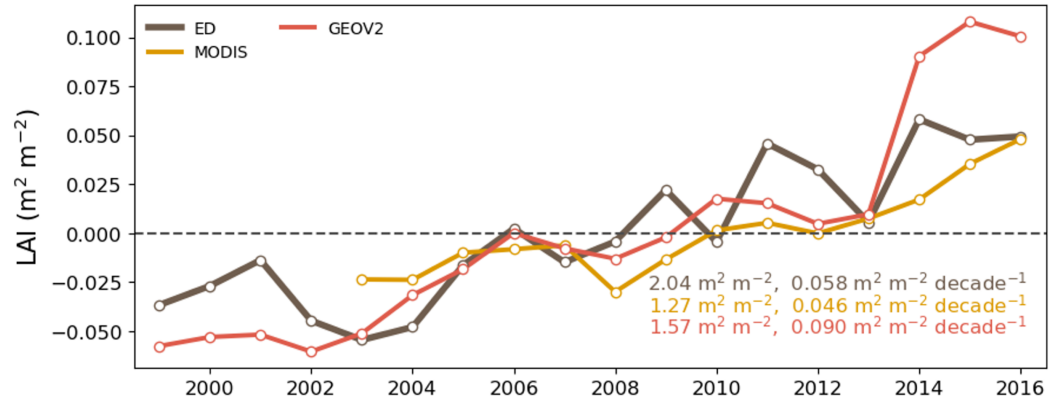


Figure 13. Interannual global average growing season LAI from ED, MODIS and GEOV2. The anomaly is calculated by subtracting annual LAI by multi-year average.

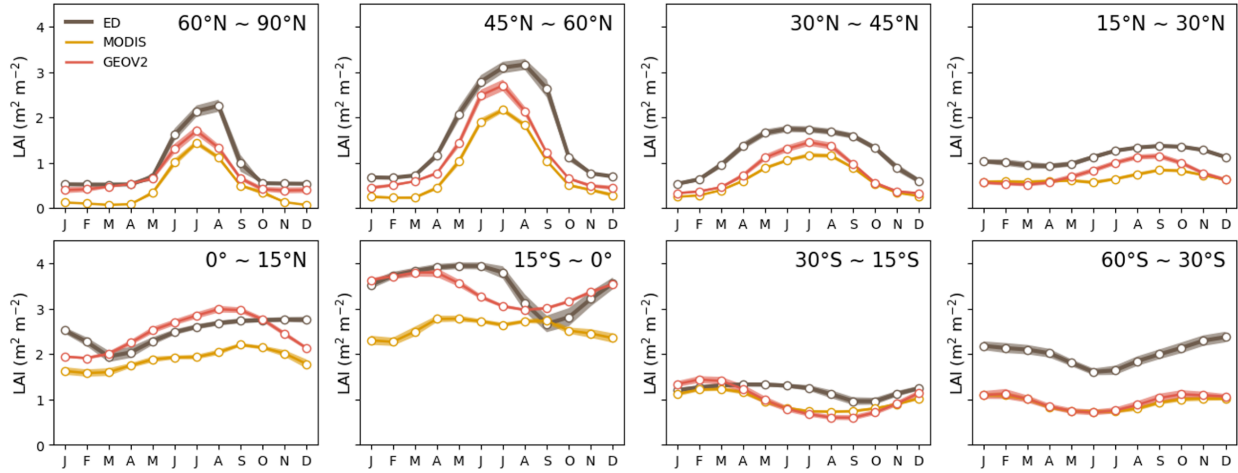


Figure 14. Seasonal LAI by latitudinal band from ED, MODIS and GEOV2.

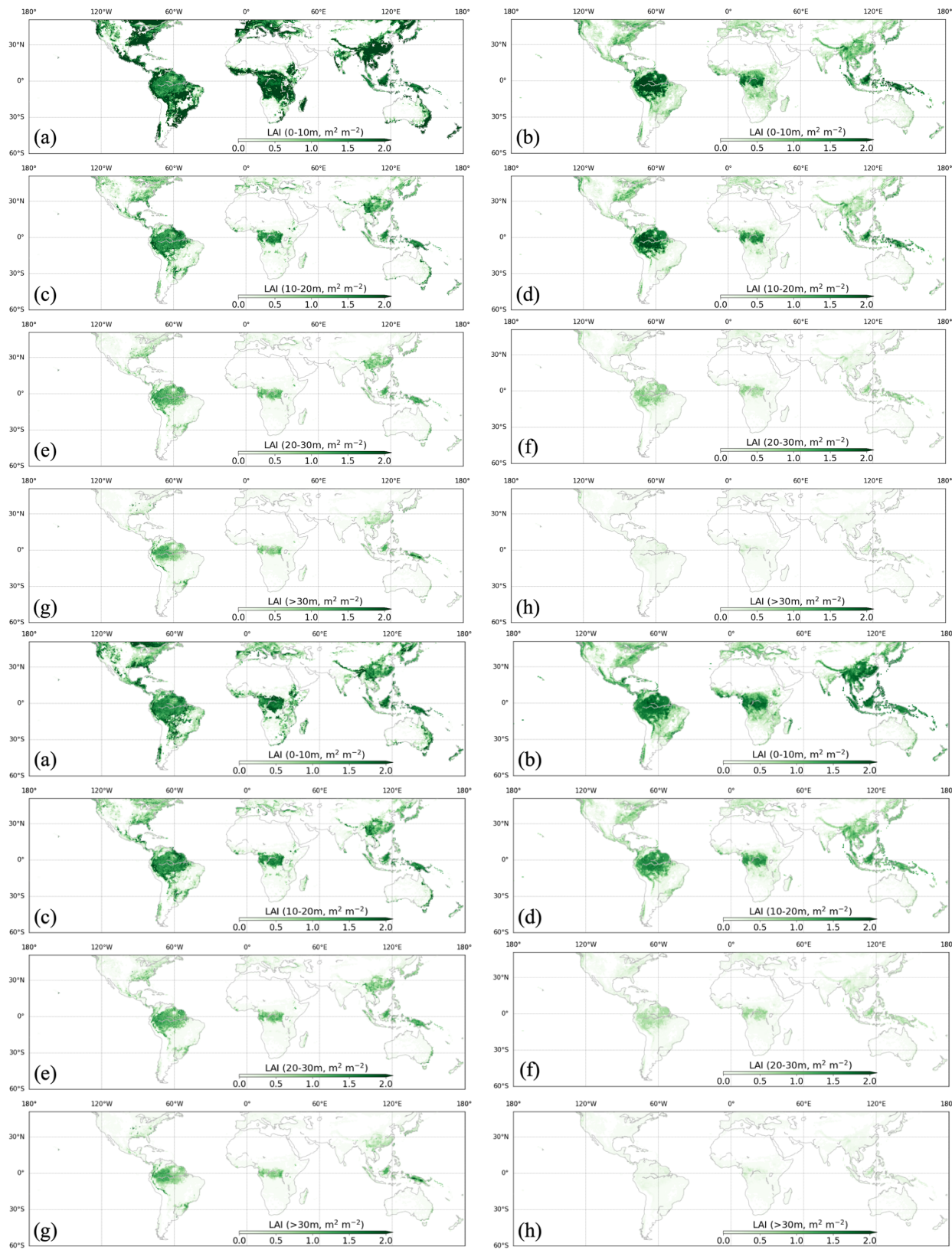
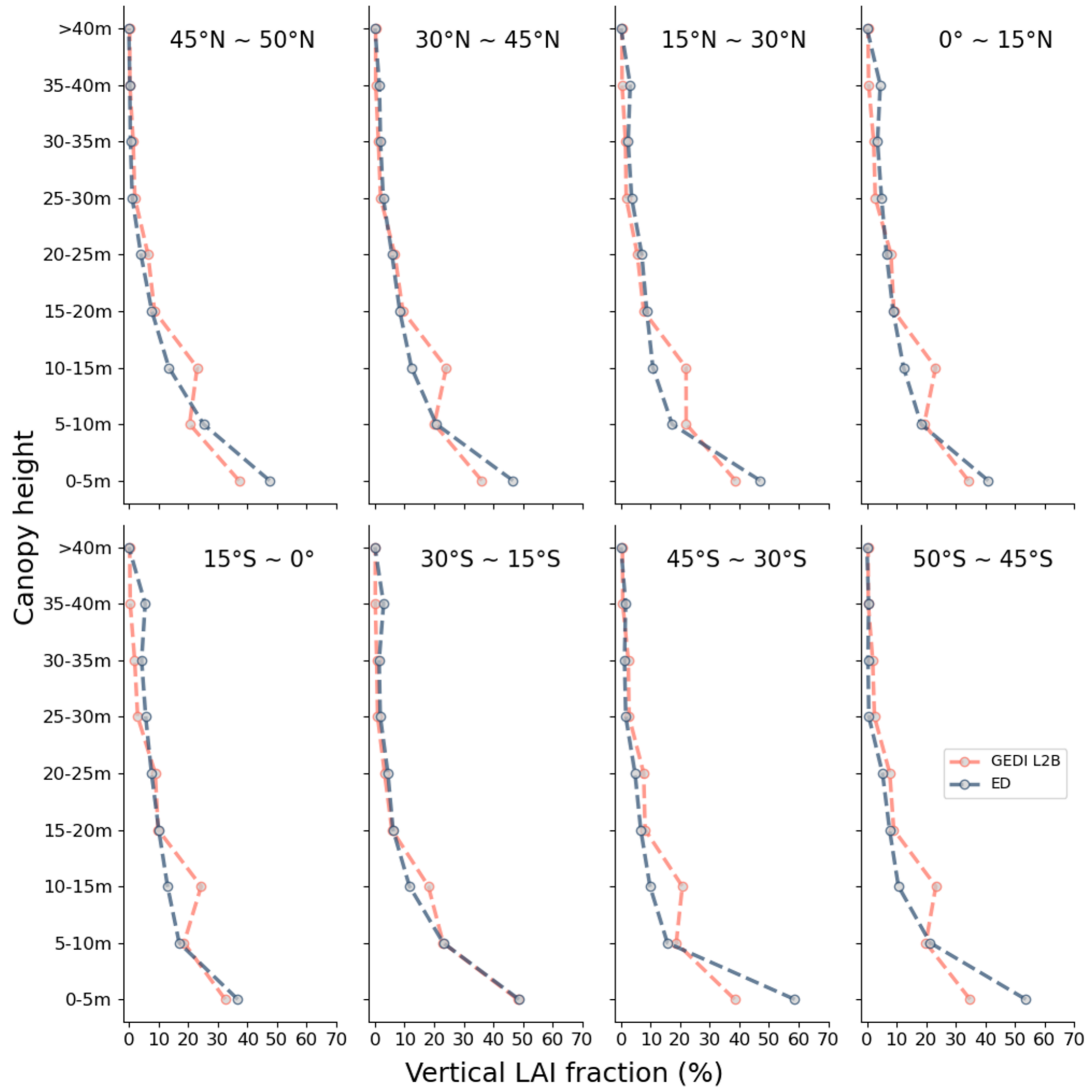


Figure 15. Vertical LAI from ED (left column) and GEDI L2B (right column) at height (0-10m) in (a) and (b), 10-20m in (c) and (d), 20-30m in (e) and (f), and above 30m in (g) and (h), respectively.



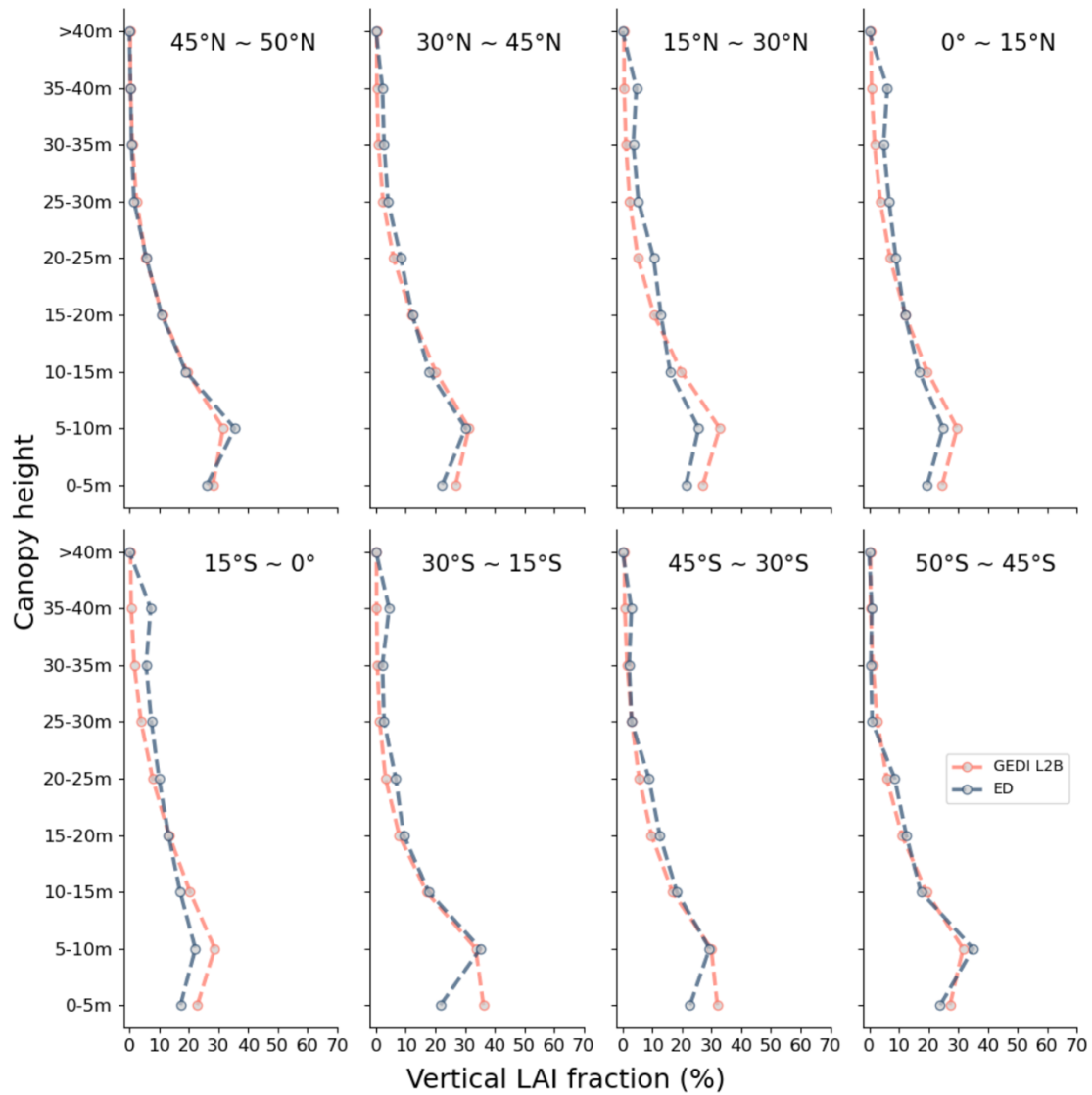


Figure 16. Relative fraction of vertical LAI by latitudinal band between ED and GEDI L2B.

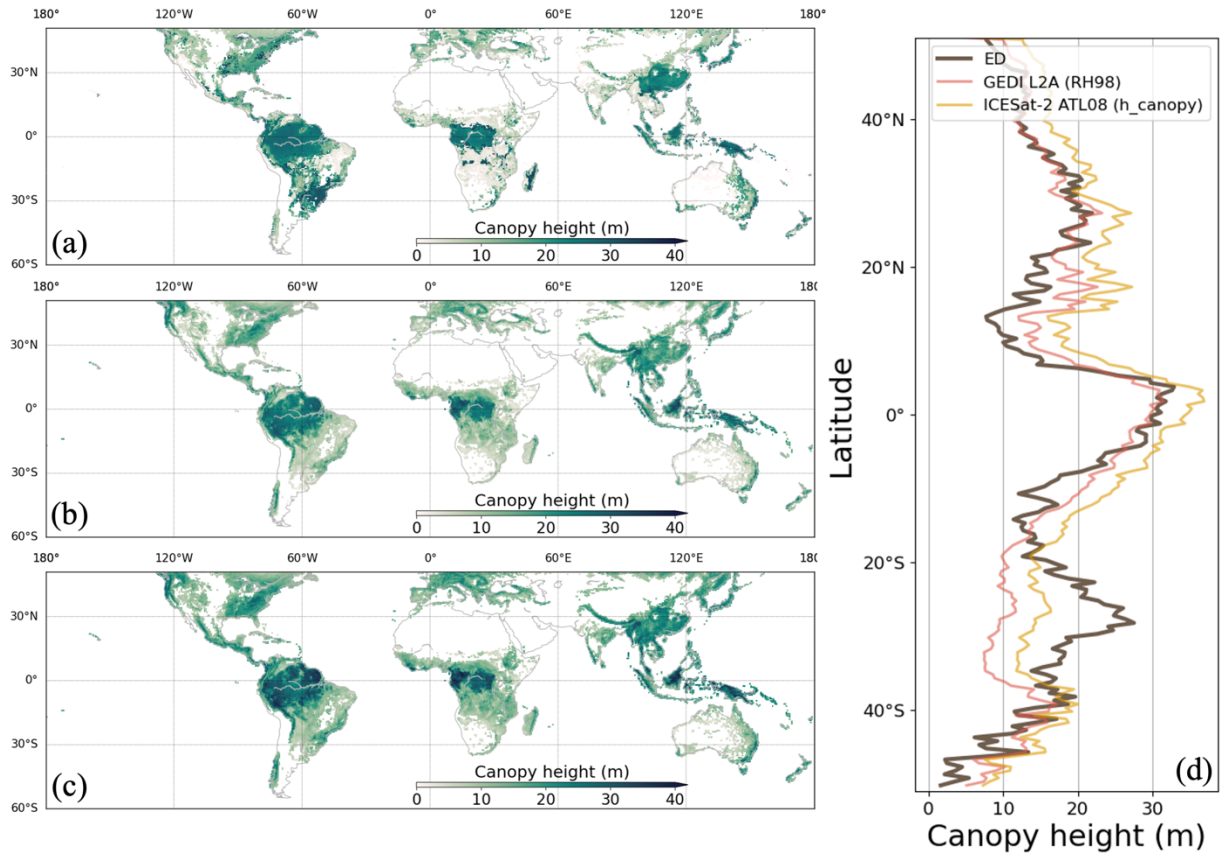
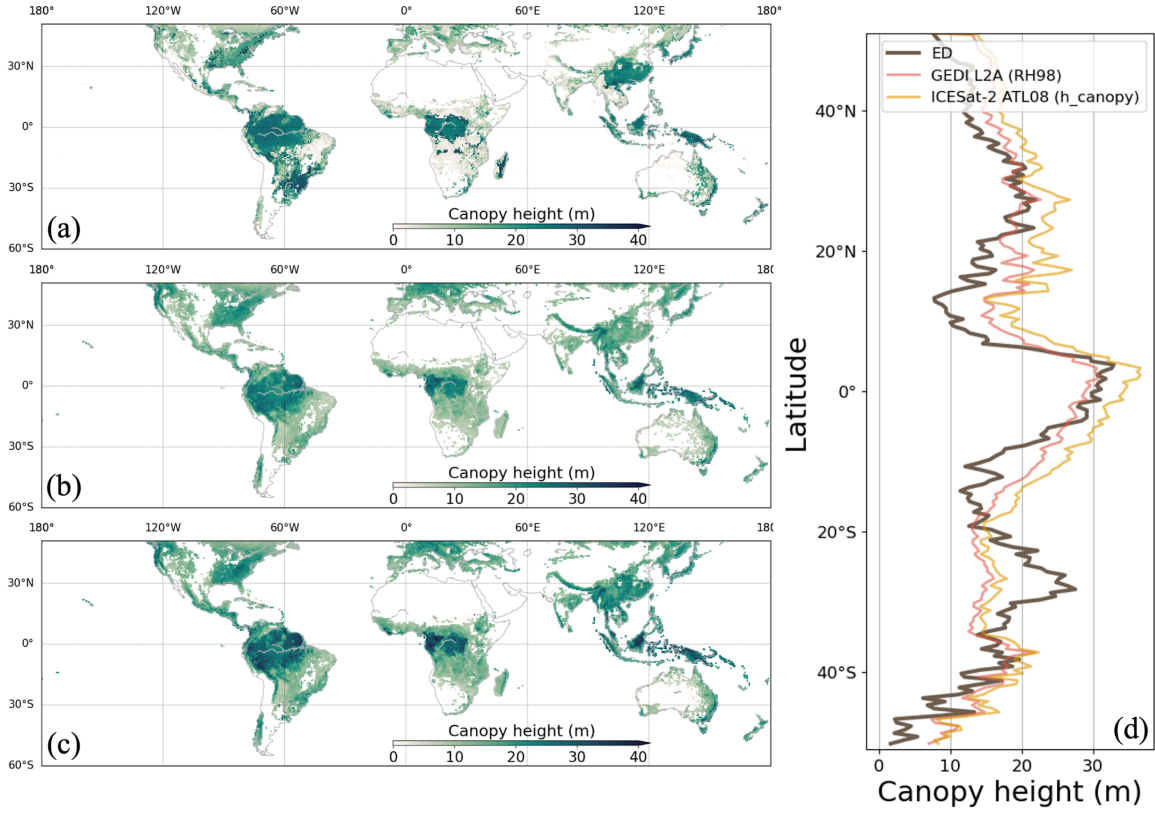


Figure 17. Canopy height from ED (a), GEDI L2A (b), and ICESat-2 ATL08 (c). Latitudinal averages are compared in (d). ESA CCI data grids with tree fractions below 5% are masked.